Nationaal Lucht- en Ruimtevaartlaboratorium
National Aerospace Laboratory NLR

NLR-TP-2001-605

Space-Time discontinuous Galerkin finite element method with dynamic grid motion for inviscid compressible flows

Efficient flux quadrature

H. van der Ven and J.J.W. van der Vegt

Nationaal Lucht- en Ruimtevaartlaboratorium
National Aerospace Laboratory NLR

NLR-TP-2001-605

Space-time discontinuous Galerkin finite element method with dynamic grid motion for inviscid compressible flows

Efficient flux quadrature

H. van der Ven and J.J.W. van der Vegt

The contents of this report have been initially prepared for publication as article in the journal Computer Methods in Applied Mechanics and Engineering, submitted December 17, 2001, to Elsevier Science, and accepted in principle for publication May 20, 2002

The second author is supported in part by a research grant form the Netherlands National Aerospace Laboratory.

Contractor:	National Aerospace Laboratory NLR
Working Plan number:	A.1.B.1
Owner:	National Aerospace Laboratory NLR
Department:	Fluid Dynamics
Distribution:	Limited
Classification title:	Unclassified
	January 2002

Summary

A new and efficient quadrature rule for the flux integrals arising in the space-time discontinuous Galerkin discretization of the Euler equations in a moving and deforming space-time domain is presented and analyzed. The quadrature rule is a factor three more efficient than the commonly applied quadrature rule and does not affect the local truncation error and stability of the numerical scheme. The local truncation error of the resulting numerical discretization is determined and is shown to be the same as when product Gauss quadrature rules are used. Details of the approximation of the dissipation in the numerical flux are presented, which render the scheme consistent and stable. The method is succesfully applied to the simulation of a three-dimensional, transonic flow over a deforming wing.

Contents

1 Table

(56 pages in total)

This page is intentionally left blank.

1 Introduction

This article discusses a new quadrature rule for the flux integrals arising in the space-time discontinuous Galerkin (DG) discretization of the unsteady Euler equations. The present article is the sequel to Van der Vegt and Van der Ven (Ref. 22) (from now on referred to as Part I), which presented the general formulation of the space-time DG method for the adaptive solution of the Euler equations in three-dimensional time-dependent flow domains. The present research is motivated by the need to apply the space-time discontinous Galerkin method to real-life (time-dependent, three-dimensional) applications. Hence, the efficiency of the numerical method immediately becomes a critical issue, especially since the DG method is known to be computationally expensive.

The computational complexity of the DG method has been investigated by various authors (Lockard and Atkins (Ref. 14), Van der Ven and Van der Vegt (Ref. 23)). The computationally most intensive part of the method is the evaluation of the flux integrals. The standard approach for the evaluation of these integrals is the application of Gauss quadrature rules. For second-order accurate space-time DG methods a mixture of two-point and three-point product rules is required, which implies twelve flux evaluations for the face fluxes and 27 flux evaluations for the volume fluxes. This number is prohibitively large and would render DG methods impractical for real-life applications.

Atkins and Shu (Ref. 2) presented a quadrature free implementation of the DG method, and in earlier work, Van der Vegt and Van der Ven (Ref. 20) presented a DG implementation which requires only one flux evaluation per face. In this latter work (Ref. 20) a slope limiter was applied for stability which subsequently was abandoned and replaced with a stabilization operator (Ref. 22). This improved both the convergence to steady state and the accuracy of the method. The quadrature rule presented in (Ref. 20), however, proved to be unstable in combination with the stabilization operator.

This prompted the development of the so-called Taylor quadrature rule, presented in this article. The Taylor quadrature rule is related to the quadrature-free approach of Atkins and Shu (Ref. 2). As in the quadrature-free approach the flux is expanded in the basis functions, but the coefficients are obtained from a direct Taylor expansion of the flux in the face center. Since the expansion coefficients of the solution vector related to the linear basis functions can be interpreted as first derivatives of the solution vector, these expansion coefficients occur directly in the Taylor expansion of the flux. This demonstrates that DG methods provide a natural setting for the Taylor quadrature rule.

For linear fluxes, this flux expansion is equal to the flux expansion in the quadrature-free approach, but for the nonlinear Euler flux the expansion is different since we only use as many terms as the number of basis functions in the DG expansion, whereas in the quadrature-free approach the expansion would also include the second order terms in the Taylor expansion. The Taylor quadrature rule significantly reduces the number of flux evaluations, reducing the flop count with respect to the required product Gauss quadrature rule. Moreover, since only data in the face center is required, the data locality of the algorithm is improved, which enhances the computational speed on cache-based computers.

The quadrature rule in the DG method must be chosen carefully, since it can negatively affect the accuracy of the DG discretization. For the TVD Runge-Kutta space DG discretization of a multi-dimensional scalar conservation law this has been analyzed by Cockburn, Hou, and Shu (Ref. 10) when Gauss quadrature rules are used for the flux integrals. In this article we analyze the accuracy of the space-time DG discretization both for the Taylor and Gauss quadrature rules. The analysis shows that the Taylor quadrature rule does not have an adverse effect on the accuracy of the DG method, which is also confirmed by the numerical experiments discussed in Section 6 and in Part I, where experimentally a global L_2 error proportional to $h^{2.5}$ was found.

Having established the accuracy of the numerical method, the next issue is the stability of the discretization. Unlike the approach of Atkins and Shu (Ref. 2), the Taylor quadrature rule does not presuppose a relatively simple numerical flux, such as the Lax-Friedrichs flux, which for our applications is too dissipative. In this article the HLLC flux (Toro (Ref. 17)) is used, which has comparable accuracy to the Osher numerical flux, at considerably less computational cost. In our experience the proper integration of the upwind dissipation of the numerical flux is also essential for the stability of the gradient equations. This implies that the dissipative part of the numerical flux must be linearized as well. The linearization of the HLLC flux in the Taylor quadrature rule is discussed in detail, and is constructed such that it results in a stable scheme, with correct treatment of the pressure term at contact discontinuities boundaries, and satisfying the Geometric Conservation Law for moving meshes.

The contents of the article is as follows. In Section 2 the space-time DG discretization of the Euler equations in a moving and deforming flow domain is summarized. In Section 3 the Taylor quadrature rule for the face flux integrals is presented. In Section 4 the details of the linearization of the dissipative part of the numerical flux are discussed, which render the scheme consistent and stable. In Section 5 the local truncation error of the DG scheme using the Taylor and Gauss quadrature rules is analyzed. Finally, in Section 6 some numerical experiments are presented,

including the flow past a three-dimensional, deforming wing.

2 Numerical method

In this section the Euler equations in a moving and deforming flow domain and their space-time discontinuous Galerkin discretization are presented. The following is a summary of Part I and will introduce the notations.

2.1 Euler equations in a moving and deforming time domain

We consider the Euler equations of gas dynamics in a time-dependent flow domain. Since the flow domain boundary is moving and deforming in time we do not make an explicit separation between the space and time variables and consider the Euler equations directly in $\mathbb{R}^4$. Let $\mathcal{E} \subset \mathbb{R}^4$ be an open domain. A point $x \in \mathbb{R}^4$ has coordinates $(x_1, \cdots, x_4)$, but we will also frequently use the notation $t = x_4$ for the time coordinate. The flow domain $\Omega(t)$ at time t, $(t_0 < t < T)$, is defined as: $\Omega(t) := \{\bar{x} \in \mathbb{R}^3 | \ (\bar{x}, t) \in \mathcal{E}\}$, with t_0 and T the initial and final time of the evolution of the flow domain. The space-time domain boundary $\partial\mathcal{E}$ consists of the hypersurfaces $\Omega(t_0) := \{x \in \partial\mathcal{E} \mid x_4 = t_0\}$, $\Omega(T) := \{x \in \partial\mathcal{E} \mid x_4 = T\}$ and $\mathcal{Q} := \{x \in \partial\mathcal{E} \mid t_0 < x_4 < T\}$. %medskip

Let $\mathcal{F} : \mathbb{R}^5 \to \mathbb{R}^{5\times 4}$ denote the flux tensor, which is defined as:

$$\mathcal{F} = \begin{pmatrix} \rho u_1 & \rho u_2 & \rho u_3 & \rho \\ \rho u_1^2 + p & \rho u_1 u_2 & \rho u_1 u_3 & \rho u_1 \\ \rho u_1 u_2 & \rho u_2^2 + p & \rho u_2 u_3 & \rho u_2 \\ \rho u_1 u_3 & \rho u_2 u_3 & \rho u_3^2 + p & \rho u_3 \\ (\rho E + p) u_1 & (\rho E + p) u_2 & (\rho E + p) u_3 & \rho E \end{pmatrix},$$

with ρ, p, and E the density, pressure, and specific total energy, respectively, and u_i the velocity components in the Cartesian coordinate directions x_i, $i \in \{1, 2, 3\}$ of the velocity vector $u : \mathcal{E} \to \mathbb{R}^3$. Let the vector $U : \mathcal{E} \to \mathbb{R}^5$ denote the conservative flow variables with components:

$$U_i = \mathcal{F}_{i4},$$

then the Euler equations of gas dynamics are defined as:

$$\operatorname{div} \mathcal{F}\big(U(x)\big) = 0, \qquad x \in \mathcal{E}, \tag{1}$$

together with the initial and boundary conditions:

$$\begin{aligned} U(x) &= U_0(x), && x \in \Omega(t_0), \\ U(x) &= \mathcal{B}(U, U_w), && x \in \mathcal{Q}. \end{aligned}$$

Here $U_0 : \Omega(t_0) \rightarrow \mathbb{R}^5$ denotes the initial flow field, $\mathcal{B} : \mathbb{R}^5 \times \mathbb{R}^5 \rightarrow \mathbb{R}^5$ the boundary operator and $U_w : \mathcal{Q} \rightarrow \mathbb{R}^5$ the prescribed boundary flow field data. The divergence of a second order tensor is defined as: $\mathrm{div}\, \mathcal{F} = \frac{\partial \mathcal{F}_{ij}}{\partial x_j}$, and the summation index is used on repeated indices in this article. The Euler equations are completed with the equation of state for a caloric perfect gas: $p = (\gamma - 1)\rho(E - \frac{1}{2}u_i u_i)$, with γ the ratio of specific heats.

In the entire article, the notation $\bar{x}$ for an arbitrary vector $x \in \mathbb{R}^4$ is used for the vector $\bar{x}$ in $\mathbb{R}^3$ with components identical to the first three components of x. As a special case, $\overline{\mathcal{F}}$ is the usual Euler flux defined by $\overline{\mathcal{F}}_{ij} = \mathcal{F}_{ij}$, $1 \leq j \leq 3$, $1 \leq i \leq 5$.

2.2 Geometry of space-time elements

Consider a partitioning $t_0 < t_1 < \cdots < t_{N_T} = T$ of the time interval (t_0, T) and define the time interval I_n as: $I_n = (t_n, t_{n+1})$. The space-time domain $\mathcal{E} \subset \mathbb{R}^4$ is split into a finite number of space-time slabs $\mathcal{E} \cap I_n$. The evolution of the flow domain during the time interval I_n is represented by the mapping Φ_t^n, which is defined as:

$$\Phi_t^n : \Omega(t_n) \rightarrow \Omega(t) : \bar{x} \mapsto \Phi_t^n(\bar{x}), \qquad t \in I_n. \tag{2}$$

The mapping Φ_t^n is assumed to be sufficiently smooth, orientation preserving and invertible in each time interval I_n, but not necessarily across time intervals.

At the time level t_n we use hexahedral elements K to define the tessellation $\bar{\mathcal{T}}_h^n$ of $\Omega(t_n)$:

$$\bar{\mathcal{T}}_h^n := \{K_j^n \mid \bigcup_{j=1}^{N_n} \bar{K}_j^n = \bar{\Omega}_h(t_n) \text{ and } K_j^n \cap K_{j'}^n = \emptyset \quad \text{if } j \neq j',\ 1 \leq j, j' \leq N_n\}.$$

Each element $K^n \in \bar{\mathcal{T}}_h^n$ is related to the master element $\hat{K} = (-1, 1)^3$ through the mapping F_K^n:

$$F_K^n : \hat{K} \rightarrow K^n : \bar{\xi} \mapsto \bar{x} = \sum_{i=1}^{8} \bar{x}_i(K^n)\chi_i(\bar{\xi}),$$

with $\bar{x}_i(K^n) \in \mathbb{R}^3$, $1 \leq i \leq 8$, the spatial coordinates of the vertices of the hexahedron K^n at time t_n and $\chi_i(\bar{\xi})$ the standard tri-linear finite element shape functions for hexahedra, with $\bar{\xi} = (\xi_1, \xi_2, \xi_3) \in \hat{K}$. The elements K^{n+1}, constituting the tesselation at the time level t_{n+1} are obtained by moving the vertices of each hexahedron $K^n \in \bar{\mathcal{T}}_h^n$ with the mapping Φ_t^n to their new position at time $t = t_{n+1}$, and we can define the mapping:

$$F_K^{n+1} : \hat{K} \rightarrow K^{n+1} : \bar{\xi} \mapsto \bar{x} = \sum_{i=1}^{8} \Phi_{t_{n+1}}^n\left(\bar{x}_i(K^n)\right)\chi_i(\bar{\xi}).$$

The space-time elements are obtained by connecting the elements in $\Omega_h(t_n)$ and $\Omega_h(t_{n+1})$ by linear interpolation in time. This results in the following parameterization of the space-time elements $\mathcal{K}^n$:

$$\begin{aligned} G_K^n :&\hat{\mathcal{K}} \rightarrow \mathcal{K}^n : \xi \mapsto (\bar{x}, t) \\ \bar{x} =&\tfrac{1}{2}(1-\xi_4)F_K^n(\bar{\xi}) + \tfrac{1}{2}(1+\xi_4)F_K^{n+1}(\bar{\xi}), \\ t =&\tfrac{1}{2}(t_n + t_{n+1}) + \tfrac{1}{2}(t_{n+1} - t_n)\xi_4, \end{aligned} \tag{3}$$

with ξ the computational coordinates in the master element $\hat{\mathcal{K}} = (-1,1)^4$. The space-time tessellation is now defined as:

$$\mathcal{T}_h^n := \{\mathcal{K} = G_K^n(\hat{\mathcal{K}}) \mid \ K \in \bar{\mathcal{T}}_h^n\}.$$

We will also frequently use the notation $K(t) = \{\bar{x} \in \mathbb{R}^3 | (\bar{x}, t) \in \mathcal{K}\}$ for the element K at time t. The space-time element $\mathcal{K}^n$ is bounded by the hypersurfaces $K(t_n^+) = \lim_{\epsilon \downarrow 0} K(t_n + \epsilon)$, $K(t_{n+1}^-) = \lim_{\epsilon \downarrow 0} K(t_{n+1} - \epsilon)$, and $\mathcal{Q}^n = \partial\mathcal{K}^n \setminus \big(K(t_n^+) \cup K(t_{n+1}^-)\big)$.

For $1 \leq m \leq 8$ define the eight faces $\mathcal{S}_m$ of an element $\mathcal{K}$ by $\mathcal{S}_{2n-1} = \{G_K(\xi) | \xi \in \hat{\mathcal{K}}, \xi_n = -1\}$, and $\mathcal{S}_{2n} = \{G_K(\xi) | \xi \in \hat{\mathcal{K}}, \xi_n = 1\}$, for $1 \leq n \leq 4$. Note that $\mathcal{S}_7 = K(t_n^+)$, $\mathcal{S}_8 = K(t_{n+1}^-)$, and $\cup_{m=1}^6 \mathcal{S}_m = \mathcal{Q}^n$.

2.3 Flow field expansion

The discontinuous Galerkin finite element discretization is obtained by approximating the flow field $U(x,t)$ and test functions $W(x,t)$ with polynomial expansions in each element $\mathcal{K}$, which are discontinuous across element faces, both in space and time. In the master element $\hat{\mathcal{K}}$ the basis functions $\hat{\phi}_m$ $(m = 0, \ldots, 4)$ are defined which are linear in space and time:

$$\hat{\phi}_m(\xi) = \begin{cases} 1, & m = 0, \\ \xi_m, & m > 0. \end{cases}$$

The basis functions ϕ_m in an element $\mathcal{K}$ are related to the basis function in the master element $\hat{\mathcal{K}}$ through the parametrization G_K: $\phi_m = \hat{\phi}_m \circ G_K^{-1}, (m = 0, \ldots, 4)$.

As explained in Part I the basis functions are slightly modified in such a way that the first expansion coefficient represents the element mean flow at time $t = t_{n+1}$. Define

$$\psi_m(\bar{x}, t) = \begin{cases} 1, & m = 0, \\ \phi_m(\bar{x}, t) - \frac{1}{|K(t_{n+1}^-)|} \int_{K(t_{n+1}^-)} \phi_m(\bar{x}, t_{n+1}^-) dK, & m = 1, \ldots, 4, \end{cases} \tag{4}$$

then we obtain the following expressions for U_h:

$$U_h(\bar{x},t) = \sum_{m=0}^{4} \hat{U}_m(\mathcal{K})\psi_m(\bar{x},t), \qquad (\bar{x},t) \in \mathcal{K}, \tag{5}$$

where

$$\hat{U}_0(\mathcal{K}) = \overline{U}(K(t_{n+1}^-)) = \frac{1}{|K(t_{n+1}^-)|}\int_{K(t_{n+1}^-)} U_h(\bar{x},t_{n+1}^-)dK.$$

Let $V_h^1(\mathcal{T}_h^n)$ be the discrete broken function space defined as

$$V_h^1(\mathcal{T}_h^n) = \{f : \mathcal{T}_h^n \to \mathbb{R}^5 | f_{|\mathcal{K}} \subset \text{span}\{\psi_m | 0 \le m \le 4\}\}.$$

2.4 Weak formulation of the Euler equations

The weak formulation of the Euler equations is obtained by multiplying the (space-time) Euler equations with a test function W_h, integrating over a space-time element $\mathcal{K}$ and using Gauss' theorem to obtain face flux integrals. Details of this derivation are given in Part I.

In order to ensure that the weak formulation of the Euler equations is well defined we introduce the broken space $V(\mathcal{T}_h^n)$:

$$\begin{aligned} V(\mathcal{T}_h^n) := \big\{ U : \mathcal{T}_h^n \to \mathbb{R}^5 \mid & (\operatorname{grad} U^1)^T : \mathcal{F}(U^2)|_{\mathcal{K}} \in L^1(\mathcal{K}); \\ & \gamma^-(U^1)\cdot\big(n_{\mathcal{K}}^T\mathcal{F}(\gamma^-(U^2)) + n_{\mathcal{K}}^T\mathcal{F}(\gamma^+(U^3))\big) \in L^1(\partial\mathcal{K}); \\ & \forall (U^1,U^2,U^3) \in V(\mathcal{T}_h^n),\ \forall \mathcal{K} \in \mathcal{T}_h^n \big\}, \end{aligned}$$

with L^1 the space of Lebesgue integrable functions, $\gamma^{\pm}(U) = \lim_{\epsilon\downarrow 0} U(x \pm \epsilon n_{\mathcal{K}})$ the traces of U at $\partial\mathcal{K}$, $n_{\mathcal{K}} \in \mathbb{R}^4$ the unit outward normal vector at $\partial\mathcal{K}$, and superscript T denoting the transposition of a vector. We will also frequently use the notation $U^{\pm}$ to denote $\gamma^{\pm}(U)$. The gradient operator $\operatorname{grad} : \mathbb{R}^5 \to \mathbb{R}^{4\times 5}$ is defined as: $(\operatorname{grad} U)_{ij} = \frac{\partial U_j}{\partial x_i}$ and the symbol : represents the dyadic product of two second order tensors and is defined for $\mathcal{A}, \mathcal{B} \in \mathbb{R}^{n\times m}$ as $\mathcal{A} : \mathcal{B} = \mathcal{A}_{ij}\mathcal{B}_{ij}$.

The weak form of the Euler equations is (compare with Equation (15) in Part I):

$$\begin{aligned} &\sum_{n=0}^{N_T}\sum_{j=1}^{N_n}\Big\{ -\int_{\mathcal{K}_j^n} (\operatorname{grad} W_h)^T : \mathcal{F}(U_h)d\mathcal{K} + \\ &\int_{K_j(t_{n+1}^-)} W_h^- \cdot U_h^- dK - \int_{K_j(t_n^+)} W_h^- \cdot U_h^+ dK + \int_{\mathcal{Q}_j^n} W_h^- \cdot H(U_h^-, U_h^+, \bar{n}_{\mathcal{K}})d\mathcal{Q}\Big\} = 0. \end{aligned} \tag{6}$$

(For clarity of presentation the stabilization operator $\mathfrak{D}$ introduced in Part I is omitted from the weak form of the Euler equations.) The numerical flux $H = H(U_h^-, U_h^+, \bar{n}_{\mathcal{K}})$ is introduced

to stabilize the central flux $\frac{1}{2}\big(\bar{n}_{\mathcal{K}}^T\tilde{\mathcal{F}}(U_h^-)+\bar{n}_{\mathcal{K}}^T\tilde{\mathcal{F}}(U_h^+)\big)$, where the ALE flux $\tilde{\mathcal{F}}$ is defined by $\tilde{\mathcal{F}}(U)=\overline{\mathcal{F}}(U)-v\otimes U$ (v the grid velocity). In this article, the HLLC flux is used (see Section 2.5).

As explained in Part I the time discontinuity at the intersection of the time slabs is treated using a time numerical flux, which is just the upwind flux. Note that this is equivalent with the usual approach where a time slab coupling term is added to the weak form of the equations. By defining the space-time numerical flux H_{SP} as

$$H_{\text{SP}}(U_h^-,U_h^+,n_{\mathcal{K}})=\begin{cases} H(U_h^-,U_h^+,\bar{n}_{\mathcal{K}}) & \text{if } \bar{n}_{\mathcal{K}}\neq 0,\\ \frac{1}{2}(U_h^-+U_h^+)n_{\mathcal{K},4}-\frac{1}{2}|n_{\mathcal{K},4}|(U_h^+-U_h^-) & \text{if } \bar{n}_{\mathcal{K}}=0,\end{cases}$$

the weak formulation (6) can be rewritten as

$$\sum_{n=0}^{N_T}\sum_{j=1}^{N_n}\Big\{-\int_{\mathcal{K}_j^n}(\operatorname{grad}W_h)^T:\mathcal{F}(U_h)d\mathcal{K}+\int_{\partial\mathcal{K}_j^n}W_h^-\cdot H_{\text{SP}}(U_h^-,U_h^+,n_{\mathcal{K}})d(\partial\mathcal{K})\Big\}=0. \tag{7}$$

This formulation will be used in Section 5 to determine the local truncation error.

The main interest of the present article are the resulting face and volume flux integrals:

$$\int_{\mathcal{Q}}\phi_l H(U_h^-,U_h^+,\bar{n}_{\mathcal{K}})d\mathcal{Q},\quad\text{and} \tag{8}$$

$$\int_{\mathcal{K}}\frac{\partial\phi_l}{\partial x_k}\overline{\mathcal{F}}_{ik}(U_h)d\mathcal{K}, \tag{9}$$

($1\le i\le 5$, $0\le l\le 4$). The evaluation of these flux integrals will be performed in a reference element, and to this end the following notation is introduced. Let $d\hat{\mathcal{S}}^m$ (resp. $d\overline{\mathcal{S}}^m$) be the $\mathbb{R}^4$ valued (resp. $\mathbb{R}^3$ valued) measure on $\hat{\mathcal{S}}=(-1,1)^3$ such that

$$\int_{\mathcal{S}_m}f n_{\mathcal{K}}dx=\int_{\hat{\mathcal{S}}}f\,d\hat{\mathcal{S}}^m,$$
$$\int_{\mathcal{S}_m}f\bar{n}_{\mathcal{K}}dx=\int_{\hat{\mathcal{S}}}f\,d\overline{\mathcal{S}}^m,$$

($1\le m\le 6$), where f is a function on $\mathcal{S}_m\subset\partial\mathcal{K}$ and dx is the Euclidean measure on $\mathcal{S}_m$. The precise expression for the two measures is given in the appendix. In the appendix it will be shown that the vector-valued measures $d\hat{\mathcal{S}}^m$ and $d\overline{\mathcal{S}}^m$ satisfy the following relation for $1\le m\le 6$:

$$\int_{\hat{\mathcal{S}}}f\cdot d\hat{\mathcal{S}}^m=\frac{1}{2}\Delta t\left(\int_{\hat{\mathcal{S}}}\overline{f}\cdot d\overline{\mathcal{S}}^m-\int_{\hat{\mathcal{S}}}f_4 v\cdot d\overline{\mathcal{S}}^m\right), \tag{10}$$

for any integrable function $f:\mathcal{S}_m\to\mathbb{R}^4$, where $v=(F_K^{n+1}-F_K^n)/\Delta t$ is the local grid velocity. Taking $f=W_h^T\mathcal{F}$ we have

$$\int_{\mathcal{S}_m}W_h^T\mathcal{F}n_{\mathcal{K}}dx=\frac{1}{2}\Delta t\left(\int_{\hat{\mathcal{S}}}W_h^T\overline{\mathcal{F}}\cdot d\overline{\mathcal{S}}^m-\int_{\hat{\mathcal{S}}}W_h^T U v\cdot d\overline{\mathcal{S}}^m\right), \tag{11}$$

in which we recognize the ALE formulation containing the grid velocity. In the remainder of this article we will drop the subscript $\mathcal{K}$ from the space-time normal n.

2.5 HLLC flux

For the numerical flux the HLLC flux (Toro (Ref. 17) and Batten et al. (Ref. 4)) is used since this technique combines well with the quadrature rule presented in the next sections. In this section the main elements of the HLLC flux will be presented, after which the flux will be transformed to a form more suitable for the flux integration.

The HLLC flux is an approximate flux for the Riemann problem of gas dynamics. Given the left and right state U_L and U_R in the Riemann problem, the HLLC flux uses two intermediate states to define the numerical flux. Given a moving face with space normal $\bar{n}$, normal velocity components $\hat{u}_L$ and $\hat{u}_R$, local speeds of sound a_L and a_R, and normal grid velocity v, let $S_L = \min(\hat{u}_L - a_L, \hat{u}_R - a_R)$ be the minimum wave speed, $S_R = \max(\hat{u}_L + a_L, \hat{u}_R + a_R)$ the maximum wave speed, and define the contact wave speed S_M as

$$S_M = \frac{\rho_R \hat{u}_R(S_R - \hat{u}_R) - \rho_L \hat{u}_L(S_L - \hat{u}_L) + p_L - p_R}{\rho_R(S_R - \hat{u}_R) - \rho_L(S_L - \hat{u}_L)}. \tag{12}$$

The intermediate pressures p_L^* and p_R^* are defined as

$$\begin{aligned} p_L^* &= \rho_L(S_L - \hat{u}_L)(S_M - \hat{u}_L) + p_L \\ p_R^* &= \rho_R(S_R - \hat{u}_R)(S_M - \hat{u}_R) + p_R. \end{aligned} \tag{13}$$

By construction of the contact wave speed S_M the intermediate pressure is constant over the contact wave: $p^* = p_L^* = p_R^*$. The HLLC flux is defined by (see Part I for details):

$$\begin{aligned} H_{\text{HLLC}}(U_L, U_R) = \tfrac{1}{2}\big(&\hat{\mathcal{F}}(U_L) + \hat{\mathcal{F}}(U_R) - (|S_L - v| - |S_M - v|)U_L^* + \\ &(|S_R - v| - |S_M - v|)U_R^* + |S_L - v|U_L - |S_R - v|U_R - \\ &v(U_L + U_R)\big), \end{aligned} \tag{14}$$

where the left intermediate state is derived as

$$\begin{aligned} U_L^* &= \frac{S_L - \hat{u}_L}{S_L - S_M}U_L + \frac{1}{S_L - S_M}\begin{pmatrix} 0 \\ (p^* - p_L)\bar{n} \\ p^* S_M - p_L \hat{u}_L \end{pmatrix} \\ &= \frac{S_L}{S_L - S_M}U_L - \frac{1}{S_L - S_M}\left[\hat{u}_L U_L + p_L \begin{pmatrix} 0 \\ \bar{n} \\ \hat{u}_L \end{pmatrix}\right] + \frac{1}{S_L - S_M}p^* \begin{pmatrix} 0 \\ \bar{n} \\ S_M \end{pmatrix} \end{aligned}$$

(right intermediate state is computed likewise). Recognizing the second term between square

brackets on the right hand side as a flux term, the HLLC flux can be rewritten as

$$\begin{aligned} H_{\mathrm{HLLC}}(U_L, U_R, n) = c_L \hat{\mathcal{F}}_L + c_R \hat{\mathcal{F}}_R - \frac{1}{2} v (U_L + U_R) \\ + \frac{1}{2}\left(|\tilde{S}_L| - S_L \frac{|\tilde{S}_L| - |\tilde{S}_M|}{S_L - S_M} \right) U_L - \frac{1}{2}\left(|\tilde{S}_R| - S_R \frac{|\tilde{S}_R| - |\tilde{S}_M|}{S_R - S_M} \right) U_R \\ - \frac{1}{2}\left(\frac{|\tilde{S}_L| - |\tilde{S}_M|}{S_L - S_M} - \frac{|\tilde{S}_R| - |\tilde{S}_M|}{S_R - S_M} \right) p^* v_p, \end{aligned} \tag{15}$$

where $\hat{\mathcal{F}}_L = \hat{\mathcal{F}}(U_L) = \overline{\mathcal{F}}(U_L) \cdot \overline{n}$ is the normal flux. The corrected wave speeds are defined as $\tilde{S}_* = S_* - v$, the constants c_L and c_R are given by the relations

$$\begin{aligned} c_L &= \frac{1}{2}\left(1 + \frac{|\tilde{S}_L| - |\tilde{S}_M|}{S_L - S_M} \right), \\ c_R &= \frac{1}{2}\left(1 - \frac{|\tilde{S}_R| - |\tilde{S}_M|}{S_R - S_M} \right), \end{aligned}$$

and the vector $v_p \in \mathbb{R}^5$ is defined by

$$v_p = \begin{pmatrix} 0 \\ \overline{n} \\ S_M \end{pmatrix}.$$

The term $\frac{1}{2}(\hat{\mathcal{F}}(U_L) + \hat{\mathcal{F}}(U_R))$ in (14) is referred to as the central part of the numerical flux, the remaining terms as the dissipative part of the numerical flux.

3 Taylor quadrature rule

In an attempt to improve the computational efficiency of the second order accurate DG method a novel approximation of the flux integrals is proposed. The flux function in the integrand is replaced by the second order Taylor series of the flux evaluated at the face center. Terms containing the gradients transversal to the face are introduced into the discretized equations, enhancing the stability of the discretized system. Moreover, second order accuracy of this Taylor approximation of the flux integrals is proved in Section 5. Based on a flop count analysis (not presented here) it is estimated that this approximation is computationally more efficient than Gauss quadrature, because of the reduction in the number of flux evaluations. Also, the locality of the required flow data (only data in the face center is required) will improve the speed of the flux quadrature algorithm.

First, we will explain the basic concept of the so-called Taylor quadrature for the face flux integrals, after which we will present the general formulation for both face and volume flux integrals. In the Taylor quadrature rule, the central part of the HLLC flux is approximated as:

$$\begin{aligned}\int_{\mathcal{S}_m} \phi_m \overline{\mathcal{F}}_{ik}(U_*)\overline{n}_k dx \approx & \overline{\mathcal{F}}_{ik}(U_*(\bar{\xi}_m)) \int_{\hat{\mathcal{S}}} \xi_m d\overline{\mathcal{S}}_k^m \\ & + \sum_{l \in I(\mathcal{S}_m)} \frac{\partial \overline{\mathcal{F}}_{ik}}{\partial U_*^j}(U_*(\bar{\xi}_m)) \frac{\partial U_*^j}{\partial \xi_l}(\bar{\xi}_m) \int_{\hat{\mathcal{S}}} \xi_l \xi_m d\overline{\mathcal{S}}_k^m,\end{aligned} \tag{16}$$

where $U_* = U_L$ or U_R, $\bar{\xi}_m$ is the computational face center of the face $\mathcal{S}_m$ defined by $\bar{\xi}_{m,i} = \pm\delta_{im}$, and $I(\mathcal{S}_m)$ is the ordered index set defined by $I(\mathcal{S}_m) = \{m_2, m_3, m_4\}$, $m_2 < m_3 < m_4$, the complement of $\{m\}$ in $\{1,2,3,4\}$. These are the first four terms in a Taylor expansion of the integrand on $\hat{\mathcal{S}}$. The remaining integrals, which depend solely on the geometry of the face, are evaluated exactly — only the flux terms are expanded in a Taylor series. The exact evaluation of the geometric terms is crucial in order to maintain the second order accuracy of the DG method.

The flow derivatives necessary for the quadrature rule can be easily computed, since in computational coordinates the solution vector U_h in cell $\mathcal{K}$, restricted to the face $\mathcal{S}_{m_1}$, can be written as

$$U_{|\mathcal{S}_{m_1}} = U(\bar{\xi}_{m_1}) + \xi_{m_2}\hat{U}_{m_2}(\mathcal{K}) + \xi_{m_3}\hat{U}_{m_3}(\mathcal{K}) + \xi_4\hat{U}_4(\mathcal{K}); \tag{17}$$

hence, the flow derivatives are equal to $\frac{\partial U}{\partial \xi_l}(\bar{\xi}_{m_1}) = \hat{U}_l$ for $l \in I(\mathcal{S}_{m_1})$. The fact that the gradients occur directly in the approximation of the face flux integrals, demonstrates that DG methods provide a natural setting for the Taylor quadrature rule.

For the general formulation of the Taylor quadrature rule for both face and volume flux integrals we return to the weak formulation (7) of the Euler equations using the space-time flux. This allows us to treat the space-time fluxes through the different element faces in a uniform way.

The first step is to transform the integrals in physical space to integrals in computational space,

$$\int_{\mathcal{Q}} W_h^- \cdot \mathcal{F}^{\pm} n^T d\mathcal{Q} = \sum_{m=1}^{8} \int_{\hat{\mathcal{S}}_m} \hat{W}_{h,i}^- \cdot \mathcal{F}_{ik}^{\pm} \, d\hat{\mathcal{S}}_k^m. \tag{18}$$

Likewise the volume flux integrals are transformed to computational space:

$$\int_{\mathcal{K}} \nabla W_h : \mathcal{F} d\mathcal{K} = \int_{\hat{\mathcal{K}}} \nabla \hat{W}_h : \mathcal{F} \, |J_{G_K}| \, d\hat{\mathcal{K}}. \tag{19}$$

Subsequently the flux in the integrand is expanded in a second order Taylor series, and the following Taylor quadrature rules for the face and volume integrals are obtained:

$$\int_{\partial\mathcal{K}} W_h^- \cdot \mathcal{F}^{\pm} \cdot n_{\mathcal{K}} d\partial\mathcal{K} \approx \sum_{m=1}^{8} \Big[\mathcal{F}_{ik}^{\pm}(\bar{\xi}_m) \int_{\hat{\mathcal{S}}} \hat{W}_{h,i}^- \, d\hat{\mathcal{S}}_k^m + \sum_{l \in I(\mathcal{S}_m)} \frac{\partial \mathcal{F}_{ik}^{\pm}(\bar{\xi}_m)}{\partial \xi_l} \int_{\hat{\mathcal{S}}} \hat{W}_{h,i}^- \, \xi_l \, d\hat{\mathcal{S}}_k^m \Big], \tag{20}$$

$$\int_{\mathcal{K}} \nabla W_h : \mathcal{F} d\mathcal{K} \approx \mathcal{F}_{ij}(0) \int_{\hat{\mathcal{K}}} \frac{\partial W_{h,i}}{\partial x_j} \, |J_{G_K}| d\hat{\mathcal{K}} + \frac{\partial \mathcal{F}_{ij}(0)}{\partial \xi_l} \int_{\hat{\mathcal{K}}} \frac{\partial W_{h,i}}{\partial x_j} \xi_l \, |J_{G_K}| d\hat{\mathcal{K}}, \tag{21}$$

with $\mathcal{F}^{\pm} = \mathcal{F}(U^{\pm})$.

In Section 5.1, Lemma 3, the conditions for the flux tensor will be given such that the approximations above are well defined.

4 Taylor approximation

For the stability of the discretization, it was found to be essential to not just expand the central part of the numerical flux, but also the dissipative part. This has been one of the main reasons to apply the HLLC flux, where one can hope to obtain reasonably simple expressions for the derivatives of the dissipative part. Note that in smooth parts of the flow field the dissipative part of the numerical flux is of higher order than the central part, hence the approximation of the face integrals of the dissipative part does not affect the local truncation error analyzed in Section 5.

This section only deals with the numerical flux through the space-time faces. The time-numerical flux, including the dissipative part of the time-numerical flux, is computed analytically, which is consistent with the Taylor quadrature rule, since the time-flux is linear.

A complete linearization of the HLLC flux would require the linearization of all wave speeds. Linearization of the wave speeds is a tedious exercise, not only because the expressions for the left and right wave speeds are complex, but also because of the upwind character of the HLLC flux. An efficient linearization of the flux integral would be a linearization where the left and right wave speeds are assumed to be constant, while retaining certain desirable properties of the HLLC flux. These properties are stability of the discretization scheme, preservation of uniform flow, and the contact wave analogy for the contact wave speed.

Such a linearization is presented below, for a given space-time face $\mathcal{S} = \mathcal{S}_m$, ($1 \leq m \leq 6$), using the following assumptions:

Assumption 1 *The wave speeds S_L and S_R are assumed constant in the face, the contact wave speed S_M is allowed to vary with the flow. Variations with respect to the face normal are ignored for all wave speeds.*

Assumption 2 *The wave speeds are computed based on the face average normal $\int_{\mathcal{S}} \overline{n} dx / |\int_{\mathcal{S}} \overline{n} dx|$.*

Assumption 3 *The face moments are approximated as $\int_{\hat{\mathcal{S}}} P J_{\mathcal{S}} d\xi \approx |\int_{\hat{\mathcal{S}}} P d\overline{\mathcal{S}}|$, for an arbitrary polynomial P on $\hat{\mathcal{S}}$, where $J_{\mathcal{S}}$ is the Jacobian of the parametrization of $\mathcal{S}$.*

Assumption 4 *The coefficients in the dissipative flux containing the contact wave speed are assumed constant.*

As will be shown in Section 4.1, the first assumption is sufficient to ensure that the intermediate

pressures are equal across the contact wave up to second order in the left and right states. In Section 4.2 it will be shown that the other assumptions are sufficient to ensure the preservation of uniform flow when the Taylor quadrature rule is used. The stability of the scheme will be demonstrated experimentally in Section 6. It is important to note that the Taylor quadrature rule puts no restriction on the specific choice of the left and right wave speeds.

Using Assumption 1 to 4 and the formulation of the HLLC flux in (15) we obtain the following approximation of the face flux integrals:

$$\int_{\mathcal{S}_m} \phi_n H^i_{\text{HLLC}}(U_L, U_R, \bar{n}) dx \approx \tag{22}$$

$$\begin{aligned}
&\frac{1}{2}\left(c_L \overline{\mathcal{F}}_{ik}(U_L(\bar{\xi}_m)) + c_R \overline{\mathcal{F}}_{ik}(U_R(\bar{\xi}_m))\right) \int_{\hat{\mathcal{S}}} \xi_n d\overline{\mathcal{S}}^m_k \\
&+ \frac{1}{2} c_L \sum_{l \in I(\mathcal{S})} \frac{\partial \overline{\mathcal{F}}_{ik}}{\partial U^j}(U_L(\bar{\xi}_m)) \hat{U}^j_{L,l} \int_{\hat{\mathcal{S}}} \xi_l \xi_n d\overline{\mathcal{S}}^m_k \\
&+ \frac{1}{2} c_R \sum_{l \in I(\mathcal{S})} \frac{\partial \overline{\mathcal{F}}_{ik}}{\partial U^j}(U_R(\bar{\xi}_m)) \hat{U}^j_{R,l} \int_{\hat{\mathcal{S}}} \xi_l \xi_n d\overline{\mathcal{S}}^m_k \\
&- \frac{1}{2} \int_{\hat{\mathcal{S}}} (U_L + U_R) \xi_n v_k d\overline{\mathcal{S}}^m_k \\
&+ \frac{1}{2}\left(|\tilde{S}_L| - S_L \frac{|\tilde{S}_L| - |\tilde{S}_M|}{S_L - S_M}\right) \int_{\hat{\mathcal{S}}} U^i_L \xi_n J_{\mathcal{S}_m} d\xi \qquad (23) \\
&- \frac{1}{2}\left(|\tilde{S}_R| - S_R \frac{|\tilde{S}_R| - |\tilde{S}_M|}{S_R - S_M}\right) \int_{\hat{\mathcal{S}}} U^i_R \xi_n J_{\mathcal{S}_m} d\xi \qquad (24) \\
&- \frac{1}{2}\left(\frac{|\tilde{S}_L| - |\tilde{S}_M|}{S_L - S_M} - \frac{|\tilde{S}_R| - |\tilde{S}_M|}{S_R - S_M}\right) \tilde{F}^i(p^*).
\end{aligned}$$

The first three terms on the right hand side of (22) follow directly from (16). In the last term the

functions $\tilde{F}^i(p^*)$ are defined as

$$\begin{aligned}
\tilde{F}^1(p^*) =& 0 \\
\tilde{F}^i(p^*) =& p^*(\bar{\xi}_m) \int_{\hat{\mathcal{S}}} \xi_n d\overline{\mathcal{S}}^m_{i-1} + \qquad\qquad (2 \le i \le 4) \\
&+ \sum_{l \in I(\mathcal{S})} \left(\frac{\partial p^*}{\partial U_L^j} \hat{U}^j_{L,l} + \frac{\partial p^*}{\partial U_R^j} \hat{U}^j_{R,l} \right) \int_{\hat{\mathcal{S}}} \xi_l \xi_n d\overline{\mathcal{S}}^m_{i-1} \\
\tilde{F}^5(p^*) =& S_M(\bar{\xi}_m) p^*(\bar{\xi}_m) \int_{\hat{\mathcal{S}}} \xi_n J_{\mathcal{S}_m} d\xi + \\
&+ \sum_{l \in I(\mathcal{S})} S_M(\bar{\xi}_m) \left(\frac{\partial p^*}{\partial U_L^j} \hat{U}^j_{L,l} + \frac{\partial p^*}{\partial U_R^j} \hat{U}^j_{R,l} \right) \int_{\hat{\mathcal{S}}} \xi_l \xi_n J_{\mathcal{S}_m} d\xi \\
&+ \sum_{l \in I(\mathcal{S})} p^*(\bar{\xi}_m) \left(\frac{\partial S_M}{\partial U_L^j} \hat{U}^j_{L,l} + \frac{\partial S_M}{\partial U_R^j} \hat{U}^j_{R,l} \right) \int_{\hat{\mathcal{S}}} \xi_l \xi_n J_{\mathcal{S}_m} d\xi,
\end{aligned}$$

which essentially is the differentiation product rule applied to $p^* v_p$ in (15). The integrals in (23) and (24) are written out using (17) and Assumption 3 for the face moments:

$$\begin{aligned}
\int_{\mathcal{S}_m} U \xi_n J_{S_m} d\xi =& U(\bar{\xi}_m) \int_{\hat{\mathcal{S}}} \xi_n J_{\mathcal{S}_m} d\xi + \sum_{l \in I(\mathcal{S})} \hat{U}_l \int_{\hat{\mathcal{S}}} \xi_l \xi_n J_{\mathcal{S}_m} d\xi \\
\approx& U(\bar{\xi}_m) \left| \int_{\hat{\mathcal{S}}} \xi_n d\overline{\mathcal{S}}^m \right| + \sum_{l \in I(\mathcal{S})} \hat{U}_l \left| \int_{\hat{\mathcal{S}}} \xi_l \xi_n d\overline{\mathcal{S}}^m \right|.
\end{aligned}$$

The grid velocity term is treated in the same way:

$$\int_{\hat{\mathcal{S}}} U \xi_n v \cdot \bar{n} J_{\mathcal{S}} d\xi = U(\bar{\xi}_m) \int_{\hat{\mathcal{S}}} \xi_n v \cdot d\overline{\mathcal{S}}^m + \sum_{l \in I(\mathcal{S})} \hat{U}_l \int_{\hat{\mathcal{S}}} \xi_l \xi_n v \cdot d\overline{\mathcal{S}}^m$$

(note that this is not an approximation). The analytical expressions for the geometric integrals $\int_{\hat{\mathcal{S}}} \xi_l \xi_n d\overline{\mathcal{S}}^m$ and $\int_{\hat{\mathcal{S}}} \xi_l \xi_n v \cdot d\overline{\mathcal{S}}^m$ are presented in Appendix C.

4.1 Contact wave analogy

The intermediate pressures defined in (13) are equal if all flow quantities are evaluated at the same point. If we assume all wave speeds to be constant in a face, we would have $\frac{\partial p_R^*}{\partial U_L} = 0$, whereas clearly $\frac{\partial p_L^*}{\partial U_L}$ is nonzero. Hence a variation in the left state would have no effect on the right intermediate pressure, so the intermediate pressures will in general not be equal across the face. Since the introduction of the contact wave analogy into the HLL flux has significantly improved the accuracy of the HLLC flux, we want to preserve the contact wave analogy within the quadrature rule. We will show that taking the variation of S_M into account, but assuming S_L and S_R constant across the face, implies that the left and right intermediate pressures are equal up to second order (compare with Batten et al. (Ref. 5)), which is consistent with the Taylor quadrature rule.

Lemma 1 *Given Assumption 1, we have*

$$(p_L^* - p_R^*)(U_L + \Delta U_L, U_R + \Delta U_R) = \mathcal{O}(|\Delta U_L|^2, |\Delta U_R|^2), \quad (|\Delta U_L|,\, |\Delta U_R| \to 0).$$

Proof. Since the intermediate pressures are equal in the face center by the construction of the contact wave speed S_M, it is sufficient to prove that the linear variations of the intermediate pressures are equal.

Define $\tilde{\rho} = \rho_R(S_R - \hat{u}_R) - \rho_L(S_L - \hat{u}_L)$. Given the definition of S_M in (12) the derivative of S_M with respect to the left state is obtained as follows:

$$\begin{aligned}
\frac{\partial S_M}{\partial U_L} =& -\frac{S_M}{\tilde{\rho}}\frac{\partial \tilde{\rho}}{\partial U_L} + \frac{1}{\tilde{\rho}}\frac{\partial}{\partial U_L}\left(-\rho_L \hat{u}_L(S_L - \hat{u}_L) + p_L\right) \\
=& -\frac{S_M}{\tilde{\rho}}\frac{\partial \tilde{\rho}}{\partial U_L} + \frac{1}{\tilde{\rho}}\frac{\partial}{\partial U_L}\left(p_L^* - \rho_L S_M(S_L - \hat{u}_L)\right) \\
=& -\frac{S_M}{\tilde{\rho}}\frac{\partial \tilde{\rho}}{\partial U_L} + \frac{1}{\tilde{\rho}}\frac{\partial p_L^*}{\partial U_L} - \frac{\rho_L(S_L - \hat{u}_L)}{\tilde{\rho}}\frac{\partial S_M}{\partial U_L} + \frac{S_M}{\tilde{\rho}}\frac{\partial \tilde{\rho}}{\partial U_L} \\
=& \frac{1}{\tilde{\rho}}\frac{\partial p_L^*}{\partial U_L} - \frac{\rho_L(S_L - \hat{u}_L)}{\tilde{\rho}}\frac{\partial S_M}{\partial U_L}
\end{aligned}$$

which is equivalent with

$$\rho_R(S_R - \hat{u}_R)\frac{\partial S_M}{\partial U_L} = \frac{\partial p_L^*}{\partial U_L}.$$

Hence,

$$\frac{\partial p_R^*}{\partial U_L} = \rho_R(S_R - \hat{u}_R)\frac{\partial S_M}{\partial U_L} = \frac{\partial p_L^*}{\partial U_L},$$

where the first equality follows directly from (13). Likewise it can be proven that the derivatives with respect to U_R are equal. □

4.2 Consistency of the approximation

Lemma 2 *Given Assumption 2 to 4, the Taylor approximation of the flux integrals preserves uniform flow. Hence the flux evaluation satisfies the Geometric Conservation Law for moving meshes.*

Proof. To prove the preservation of uniform flow, it is sufficient to show that the dissipative part of the HLLC scheme vanishes in uniform flow, since the geometric terms in the central flux are evaluated exactly.

Without loss of generality we may assume $S_L < v < S_M < S_R$. The dissipative part of the HLLC scheme is given pointwise by (compare with (15))

$$\frac{\tilde{S}_L}{S_L - S_M}\left(S_M U + p v_p - \hat{\mathcal{F}}\right),$$

where the subscripts R and L are omitted from the flow variables since $U_L = U_R = U$. For uniform flow, the contact wave speed S_M is equal to the normal velocity. With the definition of the normal in the definition of the wave speeds, Assumption 2, we have:

$$S_M = \frac{u \cdot \int_{\mathcal{S}} \overline{n} dx}{|\int_{\mathcal{S}} \overline{n} dx|},$$

hence,

$$u \cdot \int_{\mathcal{S}} \overline{n} dx = S_M \left| \int_{\mathcal{S}} \overline{n} dx \right| \overset{\text{Ass. 3}}{=} S_M \int_{\mathcal{S}} dx.$$

If we now use Assumption 4 in the first equality, we obtain

$$\begin{aligned}
\int_{\mathcal{S}} \frac{\tilde{S}_L}{S_L - S_M} \left(S_M U + p v_p - \hat{\mathcal{F}} \right) dx = \\
&= \frac{\tilde{S}_L}{S_L - S_M} \int_{\mathcal{S}} \left(S_M U + p v_p - \hat{\mathcal{F}} \right) dx \\
&= \frac{\tilde{S}_L}{S_L - S_M} (U u \cdot \int_{\mathcal{S}} \overline{n} dx + \int_{\mathcal{S}} p v_p dx - \overline{\mathcal{F}} \cdot \int_{\mathcal{S}} \overline{n} dx) \\
&= \frac{\tilde{S}_L}{S_L - S_M} (\begin{pmatrix} \rho u \cdot \int_{\mathcal{S}} \overline{n} dx \\ (\rho u u + p) \int_{\mathcal{S}} \overline{n} dx \\ (\rho E + p) u \cdot \int_{\mathcal{S}} \overline{n} dx \end{pmatrix} - \overline{\mathcal{F}} \cdot \int_{\mathcal{S}} \overline{n} dx) = 0,
\end{aligned}$$

hence, uniform flow is preserved. Combined with the exact evaluation of the geometrical coefficients this proves that the Taylor quadrature rule satisfies the Geometric Conservation Law. □

4.3 Boundary conditions

The Taylor quadrature rule described above is extended to boundary faces by consistently expanding the boundary conditions in Taylor series. Since the flux for a boundary face is computed using a right state based on the left state, the expansion only depends on the left state. To be more precise, for a specific boundary condition let $f : \mathbb{R}^5 \to \mathbb{R}^5$ define the mapping describing the dummy state as function of the left state:

$$U_R = f_w(U_L) =: \mathcal{B}(U_L, U_w),$$

then

$$\begin{aligned}
\frac{\partial}{\partial \xi_l} \overline{\mathcal{F}}(U_R) &= \frac{\partial}{\partial \xi_l} \overline{\mathcal{F}}(f_w(U_L)) \\
&= \frac{\partial \overline{\mathcal{F}}}{\partial U^k}(U_R) \frac{\partial f_w^k}{\partial U^j} \hat{U}_{L,l}^j.
\end{aligned}$$

It is natural to approximate the integrals of the dissipative flux using the Taylor expansion of f:

$$\int_{\mathcal{S}} U_R^i \phi_n dx \approx U_R^i(\bar{\xi}_m) \int_{\hat{\mathcal{S}}} \xi_n J_{\mathcal{S}} d\xi + \sum_{l \in I(\mathcal{S})} \frac{\partial f_w^i}{\partial U^j} \hat{U}_{L,l}^j \int_{\hat{\mathcal{S}}} \xi_l \xi_n J_{\mathcal{S}} d\xi$$

The above two formulas show that the Taylor quadrature rule for boundary faces is equal to the Taylor quadrature rule for internal faces if we define:

$$\hat{U}_{R,l}^i = \frac{\partial f_w^i}{\partial U^j} \hat{U}_{L,l}^j. \tag{25}$$

It is straightforward to expand the boundary conditions into a Taylor series. For the slip wall boundary condition for strongly curved surfaces it may be beneficial to incorporate the variation of the face normal and grid velocity.

5 Local truncation error

In this section we will analyze the accuracy of the Taylor and Gauss quadrature rules for the flux integration. Gauss quadrature rules were used in Part I but are computationally expensive in comparison with the Taylor quadrature rules. The main result, Proposition 1, provides an estimate for the truncation error of the space-time discontinuous Galerkin discretization, including the effect of the Taylor quadrature rules. The analysis shows that the Taylor quadrature rules result in the same truncation error for the space-time DG discretization of the conservation laws, when linear test and trial functions in the reference element are used, as is obtained with the Gauss quadrature rules used in Part I. Both quadrature rules result in a second order truncation error of the discretization in the same properly chosen norm. Also, conditions on the flux tensor $\mathcal{F}$, and implicitly also on U, are given which guarantee the applicability of the Taylor and Gauss quadrature rules. These conditions and the error estimates require a high degree of smoothness. The required smoothness is, however, not available when discontinuities are present in the flow, but in these areas the numerical discretization will have a reduced accuracy anyway, independent of the quadrature rule. Definitions of the various Sobolev spaces and (semi)-norms used in this section can be found in Appendix A.

5.1 Validity of the approximation

Sufficient conditions on the flux tensor such that the Taylor quadrature rules (20) and (21) are applicable are given by the following lemma:

Lemma 3 *Let $G_K : \hat{\mathcal{K}} \to \mathcal{K}$ be a C^1 diffeomorphism for all $\mathcal{K} \in \mathcal{T}_h^n$. If $\mathcal{F} \in \left(W_B^{s,q}(\mathcal{T}_h^n)\right)^{5\times 4}$, with $s, q \in \mathbb{R}$, $1 \leq q < \infty$, s integer when $q = 1$, and $(s-1)q > 4$, then the Taylor quadrature rules presented in (20) and (21) are well defined.*

Proof. The proof of this lemma is immediate using a Taylor series expansion of the traces $\mathcal{F}^{\pm}$ and the flux tensor $\mathcal{F}$, if we can ensure that we can consider pointwise values of $\mathcal{F}^{\pm}$ at $\partial\hat{\mathcal{K}}$ and $\mathcal{F}$ in $\hat{\mathcal{K}}$, and also for their derivatives. This requires that we can imbed the flux tensor $\mathcal{F}$ in $C^1(\bar{\hat{\mathcal{K}}})$, the space of continuously differentiable functions on $\bar{\hat{\mathcal{K}}}$, the closure of $\hat{\mathcal{K}}$. Since $\hat{\mathcal{K}}$ is a bounded domain with the cone property (see Appendix A) and $(s-1)q > \dim(\hat{\mathcal{K}}) = 4$, with $s \in \mathbb{R}$ and $1 \leq q < \infty$, s integer when $q = 1$, the following imbedding exists:

$$W^{s,q}(\hat{\mathcal{K}}) \hookrightarrow C^1(\bar{\hat{\mathcal{K}}}). \tag{26}$$

For integer values of s this is part of the Rellich-Kondrachov theorem, see Adams (Ref. 1) Theorem 6.2 part II, page 144. For fractional order spaces, with s not an integer and $1 < q < \infty$, this is a direct consequence of Theorem 4.6.1/6 in Triebel (Ref. 18), pages 327–328, using the relation

between fractional order Sobolev spaces and Besov spaces, see Triebel (Ref. 18), page 323 and also Nikol'skii (Ref. 16). This means that pointwise values of $\mathcal{F}$ and its derivatives exist and the quadrature rules (20)-(21) are well defined, because the Jacobian J_{G_K} is finite when G_K is a C^1 diffeomorphism. □

Remark 1 *For the error estimates in Section 5.2 we must know to which Sobolev space the traces $\mathcal{F}^{\pm}$ belong. The imbedding theorem (26) ensures that $\mathcal{F}^{\pm} \in C^1(\hat{\mathcal{S}}_m)$, but we can also apply the imbedding theorem directly to $\hat{\mathcal{S}}_m$. If we compare the imbedding conditions $(s-1)q > 4$ for $\mathcal{F}$ in the domain $\hat{\mathcal{K}}$ and the equivalent condition $(s'-1)q > 3$ for the imbedding of $\mathcal{F}^{\pm}$ in $\hat{\mathcal{S}}_m$, then we see that $\mathcal{F}^{\pm} \in W^{s-1/q,q}(\hat{\mathcal{S}}_m)$. This result can also be obtained from the trace theorem when $s-1/q$ is not an integer, see Grisvard (Ref. 12). In the present analysis also integer values $s-1/q$ are required and we need to use (26) to determine the Sobolev spaces for $\mathcal{F}^{\pm}$.*

5.2 Analysis of element face quadrature errors

Combining (18) and (20) we can now define the quadrature error functional $E_{\partial\mathcal{K}}$ for the integration of the element face fluxes at $\partial\mathcal{K}$ as:

$$E_{\partial\mathcal{K}}(W_h^-, \mathcal{F}^{\pm}) = \sum_{m=1}^{8} \int_{\hat{\mathcal{S}}_m} \hat{W}_{h,i}^-(\xi) \Big(\mathcal{F}_{ik}^{\pm}(\xi) - \mathcal{F}_{ik}^{\pm}(\bar{\xi}_m) - \sum_{l \in I(\mathcal{S}_m)} \xi_l \frac{\partial \mathcal{F}_{ik}^{\pm}(\bar{\xi}_m)}{\partial \xi_l} \Big) d\hat{\mathcal{S}}_k^m. \qquad (27)$$

An upper bound for the quadrature error of the flux integrals over $\partial\mathcal{K}$ is provided by the following lemma:

Lemma 4 *Let the tessellation $\mathcal{T}_h^n$ satisfy the condition $0 < h_{\mathcal{T}} \leq 1$, with $h_{\mathcal{T}}$ the diameter of the smallest ball containing the elements $\mathcal{K} \in \mathcal{T}_h^n$. Suppose that for all $\mathcal{K} \in \mathcal{T}_h^n$ the mapping G_K is a C^1 diffeomorphism with $|J_{G_K^{-1}}| \leq C/h_{\mathcal{K}}^4$. Let $\mathcal{F} \in \left(W_B^{s,q}(\mathcal{T}_h^n)\right)^{5\times 4}$, with $s, q \in \mathbb{R}$, $1 \leq q < \infty$, s integer when $q = 1$, $(s-1)q > 4$, $(s-2)q \geq 1$, and $W_h \in V_h^1(\mathcal{T}_h^n)$, then the quadrature error $|E_{\partial\mathcal{K}}|$ can be estimated for all $\mathcal{K} \in \mathcal{T}_h^n$ as:*

$$|E_{\partial\mathcal{K}}(W_h^-, \mathcal{F}^{\pm})| \leq C h_{\mathcal{T}}^{2-1/p} |\mathcal{F}^{\pm}|_{2,q,\partial\mathcal{K}} \| W_h \|_{1,p,\mathcal{K}},$$

with $\frac{1}{p} + \frac{1}{q} = 1$, and C a positive constant independent of $h_{\mathcal{T}}$, $\mathcal{F}^{\pm}$ and W_h, but dependent on the grid velocity.

Remark 2 *The bound on the inverse of the Jacobian of G_K^{-1} stated in Lemma 4 is trivial for a square hexahedral space-time element and also valid for mappings close to the identity. Geometric conditions to ensure this condition for general elements are discussed in van der Vegt (Ref. 19).*

Proof. Using the triangle inequality in (27) we obtain the following estimate:

$$
\begin{aligned}
&|E_{\partial\mathcal{K}}(W_h^-, \mathcal{F}^\pm)| \\
&\qquad \leq \sum_{m=1}^{8} \int_{\hat{\mathcal{S}}_m} |\hat{W}_{h,i}^-(\xi)|\, |\mathcal{F}_{ik}^\pm(\xi) - \mathcal{F}_{ik}^\pm(\bar{\xi}_m) - \sum_{l \in I(\mathcal{S}_m)} \xi_l \frac{\partial \mathcal{F}_{ik}^\pm(\bar{\xi}_m)}{\partial \xi_l}|\, |d\hat{\mathcal{S}}_k^m| \\
&\qquad \leq C h_{\mathcal{T}}^3 \parallel \hat{W}_h^- \parallel_{0,\infty,\hat{\mathcal{S}}} \parallel \mathcal{F}^\pm \parallel_{1,\infty,\hat{\mathcal{S}}},
\end{aligned}
$$

where we used in the second step the estimate $|\xi| \leq \sqrt{3}$ for $\xi \in \hat{\mathcal{S}}_m$, and

$$
\begin{aligned}
\int_{\hat{\mathcal{S}}_m} |d\hat{\mathcal{S}}^m| &\leq \frac{1}{2}\Delta t \left(\int_{\hat{\mathcal{S}}_m} |d\bar{\mathcal{S}}^m| + \int_{\hat{\mathcal{S}}_m} |v \cdot d\bar{\mathcal{S}}^m| \right) \\
&\leq C \Delta t h_{\mathcal{T}}^2 \leq C h_{\mathcal{T}}^3, \qquad\qquad \text{for } m = 1, \cdots, 6,
\end{aligned}
$$

which can be obtained directly from the geometric integrals discussed in Appendix C. The estimates for the integrals over $\mathcal{S}_7$ and $\mathcal{S}_8$ follow directly from Appendix C. The constant C depends on the grid velocity v. We also used the fact that $\mathcal{F}^\pm \in W^{1,\infty}(\hat{\mathcal{S}})$. This is a direct consequence of the imbedding (26), which is applicable since $(s-1)q > 4$ and the relation $C^1(\bar{\hat{\mathcal{K}}}) \hookrightarrow W^{1,\infty}(\bar{\hat{\mathcal{K}}})$. This implies, as discussed in Remark 1, that $\mathcal{F}^\pm \in W^{s-1/q,q}(\hat{\mathcal{S}}) \hookrightarrow W^{1,\infty}(\hat{\mathcal{S}})$ and we obtain the estimate:

$$
|E_{\partial\mathcal{K}}(W_h^-, \mathcal{F}^\pm)| \leq C h_{\mathcal{T}}^3 \parallel \hat{W}_h^- \parallel_{0,\infty,\hat{\mathcal{S}}} \parallel \mathcal{F}^\pm \parallel_{s-1/q,q,\hat{\mathcal{S}}} .
$$

We can further improve the estimate for $|E_{\partial\mathcal{K}}|$ using the generalized Bramble-Hilbert lemma, see Bramble and Hilbert (Ref. 7).

First assume that $s - 1/q = 2$. Define the set of polynomials Q_k, such that $\frac{\partial^{k+1} q}{\partial \xi_j^{k+1}} = 0$ for $j = 1, \cdots, 4$. For any fixed $W_h(x) = \hat{W}_h(F_{\mathcal{S}}(\xi)) \in (W^{m,q}(\hat{\mathcal{S}}))^5$, with $m \geq 0$, integer, the bounded linear functional $E_{\partial\mathcal{K}}$ satisfies the relation:

$$
E_{\partial\mathcal{K}}(W_h^-, \mathcal{F}^\pm) = 0, \qquad \forall \mathcal{F}^\pm \in (Q_1(\hat{\mathcal{S}}))^{5\times 4}.
$$

The Bramble-Hilbert lemma (Ref. 7) then states that there is a positive constant $C(\hat{\mathcal{S}})$, such that for all $\mathcal{F}^\pm \in (W^{2,q}(\hat{\mathcal{S}}))^{5\times 4}$, we have the inequality:

$$
|E_{\partial\mathcal{K}}(W_h^-, \mathcal{F}^\pm)| \leq C(\hat{\mathcal{S}}) \parallel E_{\partial\mathcal{K}} \parallel_{2,q,\hat{\mathcal{S}}}^* [\mathcal{F}^\pm]_{2,q,\hat{\mathcal{S}}}, \tag{28}
$$

with:

$$
\parallel E_{\partial\mathcal{K}} \parallel_{2,q,\hat{\mathcal{S}}}^* := \sup_{0 \neq \mathcal{F}^\pm \in (W^{2,q}(\hat{\mathcal{S}}))^{5\times 4}} \frac{|E_{\partial\mathcal{K}}(W_h^-, \mathcal{F}^\pm)|}{\parallel \mathcal{F}^\pm \parallel_{2,q,\hat{\mathcal{S}}}}.
$$

The semi-norms $[\mathcal{F}^{\pm}]_{2,q,\hat{\mathcal{S}}_m}$, $1 \leq m \leq 8$, can be expressed as a semi-norm with respect to $\mathcal{S}_m$ using the following inequality (Ciarlet (Ref. 9), p. 246):

$$[\mathcal{F}^{\pm}]_{2,q,\hat{\mathcal{S}}_m} \leq C|J_{F_{\mathcal{S}}^{-1}}|^{1/q}_{0,\infty,\mathcal{S}_m}\big(|[F_{\mathcal{S}}]|^2_{1,\infty,\hat{\mathcal{S}}_m}|\mathcal{F}^{\pm}|_{2,q,\mathcal{S}_m} + |[F_{\mathcal{S}}]|_{2,\infty,\hat{\mathcal{S}}_m}|\mathcal{F}^{\pm}|_{1,q,\mathcal{S}_m}\big). \tag{29}$$

The semi-norms $|[F_{\mathcal{S}}]|_{k,\infty,\hat{\mathcal{S}}_m}$, $k \in \{1,2\}$ can be directly estimated from the isoparametric mapping G_K:

$$|[F_{\mathcal{S}}]|_{1,\infty,\hat{\mathcal{S}}_m} \leq Ch_{\mathcal{T}}, \tag{30}$$

$$|[F_{\mathcal{S}}]|_{2,\infty,\hat{\mathcal{S}}_m} = 0. \tag{31}$$

Introducing (29)-(31) into (28) and using the assumption on the Jacobian of G_K^{-1}, restricted to $\mathcal{S}$, as stated in Lemma 4, we obtain an improved estimate for $|E_{\partial\mathcal{K}}|$:

$$|E_{\partial\mathcal{K}}(W_h^-, \mathcal{F}^{\pm})| \leq Ch_{\mathcal{T}}^{5-3/q}|\mathcal{F}^{\pm}|_{2,q,\partial\mathcal{K}} \parallel \hat{W}_h^- \parallel_{0,\infty,\hat{\mathcal{S}}}, \tag{32}$$

where the positive constant C is independent of $h_{\mathcal{T}}$, $\mathcal{F}^{\pm}$ and $\hat{W}_h$, but depends on the grid velocity.

For $(s-2)q \geq 1$ we have $W^{s-1/q,q}(\hat{\mathcal{S}}) \subseteq W^{2,q}(\hat{\mathcal{S}})$, which implies that inequality (32) is also valid for $\mathcal{F}^{\pm} \in W^{s-1/q,q}(\hat{\mathcal{S}})$. This provides more flexibility to choose optimal values of s and q in the estimates for the truncation error discussed later, but does not improve the Bramble-Hilbert estimate.

The test functions W_h are chosen from the finite dimensional space $V_h^1(\mathcal{T}_h^n)$, which implies that $W_h \in (W_B^{t,p}(\mathcal{T}_h^n))^5$ with $t \geq 1$ and $\frac{1}{p} + \frac{1}{q} = 1$, because $\mathcal{F} \in (W_B^{s,q}(\mathcal{T}_h^n))^{5\times 4}$. Since all norms are equivalent in a finite dimensional space we can use a homogeneity argument (see Brenner and Scott (Ref. 8)) to obtain the following inequality:

$$\begin{aligned} \parallel \hat{W}_h \parallel_{1,\infty,\hat{\mathcal{K}}} &\leq C|J_{G_K^{-1}}|^{1/p}_{0,\infty,\mathcal{K}}\big(\parallel W_h \parallel_{0,p,\mathcal{K}} + |G_K|_{1,\infty,\hat{\mathcal{K}}}|W_h|_{1,p,\mathcal{K}}\big) \\ &\leq Ch_{\mathcal{T}}^{-4/p} \parallel W_h \parallel_{1,p,\mathcal{K}}, \qquad \text{if } 0 < h_{\mathcal{T}} \leq 1. \end{aligned} \tag{33}$$

Together with the trace theorem, we can use (33) to obtain the following estimate for $|E_{\partial\mathcal{K}}|$:

$$\begin{aligned} |E_{\partial\mathcal{K}}(W_h^-, \mathcal{F}^{\pm})| &\leq Ch_{\mathcal{T}}^{5-3/q}|\mathcal{F}^{\pm}|_{2,q,\partial\mathcal{K}} \parallel \hat{W}_h^- \parallel_{0,\infty,\hat{\mathcal{S}}} \\ &\leq Ch_{\mathcal{T}}^{5-3/q}|\mathcal{F}^{\pm}|_{2,q,\partial\mathcal{K}} \parallel \hat{W}_h \parallel_{1,\infty,\hat{\mathcal{K}}} \\ &\leq Ch_{\mathcal{T}}^{2-1/p}|\mathcal{F}^{\pm}|_{2,q,\partial\mathcal{K}} \parallel W_h \parallel_{1,p,\mathcal{K}}, \end{aligned} \tag{34}$$

with $0 < h_{\mathcal{T}} \leq 1$. In the last step we used the relation $\frac{1}{p} + \frac{1}{q} = 1$. □

In Part I we use a product Gauss quadrature rule to approximate (18). A two-point quadrature rule is applied for the three spatial computational coordinates ξ_1, ξ_2 and ξ_3, and a three-point quadrature rule for the temporal computational coordinate ξ_4. Define the quadrature error functional $E^G_{\partial\mathcal{K}}$ for the integration of the element face fluxes at $\partial\mathcal{K}$ in the same way as $E_{\partial\mathcal{K}}$ in (27) with the Taylor quadrature rule replaced with the product Gauss quadrature rule. An upper bound for the quadrature error of the flux integrals over $\partial\mathcal{K}$ using the product Gauss quadrature rule is provided by the following lemma:

Lemma 5 *Let the tessellation $\mathcal{T}_h^n$ be as in Lemma 4. Let $\mathcal{F} \in \left(W_B^{s,q}(\mathcal{T}_h^n)\right)^{5\times 4}$, with $s, q \in \mathbb{R}$, $1 \leq q < \infty$, s integer when $q = 1$, $sq > 4$, $(s-2)q \geq 1$, and $W_h \in V_h^1(\mathcal{T}_h^n)$, then the quadrature error $|E^G_{\partial\mathcal{K}}|$ can be estimated for all $\mathcal{K} \in \mathcal{T}_h^n$ as:*

$$|E^G_{\partial\mathcal{K}}(W_h^-, \mathcal{F}^\pm)| \leq C h_{\mathcal{T}}^{2-1/p} |\mathcal{F}^\pm|_{2,q,\partial\mathcal{K}} \parallel W_h \parallel_{1,p,\mathcal{K}},$$

with $\frac{1}{p} + \frac{1}{q} = 1$, and C a positive constant independent of $h_{\mathcal{T}}$, $\mathcal{F}^\pm$ and W_h, but dependent on the grid velocity.

Proof. Given the expressions of the geometric quantities in Appendix C, the product Gauss quadrature rule with two points in the spatial directions and three in the temporal direction is exact if $\hat{W}_h \in (Q_1(\hat{\mathcal{S}}))^5$ and $\mathcal{F}^\pm \in (Q_1(\hat{\mathcal{S}}))^{5\times 4}$ and we can apply the Bramble-Hilbert lemma in the same way as for Lemma 4. The remaining part of the proof is nearly identical to Lemma 4 and is not repeated here. □

Remark 3 *The product Gauss quadrature rule with two points in the spatial directions and three in the temporal direction uses the minimum number of quadrature points in a product Gauss quadrature rule necessary to satisfy the requirements of the Bramble-Hilbert lemma, which is used in the proof of Lemma 5.*

Remark 4 *Since the Gauss quadrature rule does not use derivatives we can relax the condition $(s-1)q > 4$ to $sq > 4$ to ensure the validity of the quadrature rule. For more details, see Lemma 3.*

5.3 Analysis of element volume quadrature error

The quadrature error functional $E_{\mathcal{K}}$ for the integration of the element volume fluxes can be defined as:

$$E_{\mathcal{K}}(W_h, \mathcal{F}) = \int_{\hat{\mathcal{K}}} \frac{\partial W_{h,i}}{\partial x_j} \Big(\mathcal{F}_{ij}(\xi) - \mathcal{F}_{ij}(0) - \xi_l \frac{\partial \mathcal{F}_{ij}(0)}{\partial \xi_l} \Big) |J_{G_K}| d\hat{\mathcal{K}} \tag{35}$$

using (19) and (21). The following lemma provides an upper bound for the error in the approximation of the volume flux integrals:

Lemma 6 *Let the tessellation $\mathcal{T}_h^n$ be as in Lemma 4. Let $\mathcal{F} \in \left(W_B^{s,q}(\mathcal{T}_h^n)\right)^{5\times 4}$, with $s, q \in \mathbb{R}$, $1 \leq q < \infty$, $(s-1)q > 4$, $(s-2)q \geq 1$, s integer when $q = 1$, and $W_h \in V_h^1(\mathcal{T}_h^1)$, then the quadrature error $|E_\mathcal{K}|$ can be estimated for all $\mathcal{K} \in \mathcal{T}_h^n$ as:*

$$|E_\mathcal{K}(W_h, \mathcal{F})| \leq C h_\mathcal{T}^{6-4/q} |\mathcal{F}|_{2,q,\mathcal{K}_j^n} \parallel W_h \parallel_{1,p,\mathcal{K}}, \tag{36}$$

with $\frac{1}{p} + \frac{1}{q} = 1$, and C a constant independent of h_k, $\mathcal{F}$ and W_h.

Proof. The quadrature error $E_\mathcal{K}(W_h, \mathcal{F})$ can be estimated as:

$$\begin{aligned} |E_\mathcal{K}(W_h, \mathcal{F})| \leq & \int_{\hat{\mathcal{K}}} \left| \frac{\partial W_{h,i}}{\partial x_j} \right| \left| \mathcal{F}_{ij}(\xi) - \mathcal{F}_{ij}(0) - \xi_l \frac{\partial \mathcal{F}_{ij}(0)}{\partial \xi_l} \right| |J_{G_K}| d\hat{\mathcal{K}} \\ \leq & C h_\mathcal{T}^4 \parallel \mathcal{F} \parallel_{1,\infty,\hat{\mathcal{K}}} \parallel W_h \parallel_{1,\infty,\mathcal{K}} \\ \leq & C h_\mathcal{T}^4 \parallel \mathcal{F} \parallel_{s,q,\hat{\mathcal{K}}} \parallel W_h \parallel_{1,\infty,\mathcal{K}}, \end{aligned}$$

where we used the imbedding (26), which is valid since $(s-1)q > 4$. In addition we used fact that $|\xi| \leq 2$ for $\xi \in \hat{\mathcal{K}}$ and the estimate $\int_{\hat{\mathcal{K}}} |J_{G_K}| d\hat{\mathcal{K}} \leq C h_\mathcal{T}^4$, which can be obtained directly from the geometric integrals discussed in the appendix.

The estimate of the quadrature error functional can be improved with the generalized Bramble-Hilbert lemma (Ref. 7). Due to the close resemblance with the analysis for $E_{\partial\mathcal{K}}$ only the main steps will be discussed. For any fixed value of $W_h \in (W^{m,q}(\mathcal{K}))^5$ with $m \geq 1$, the bounded linear functional $E_\mathcal{K}$ satisfies the relation:

$$E_\mathcal{K}(W_h, \mathcal{F}) = 0, \qquad \forall \mathcal{F} \in (Q_1(\hat{\mathcal{K}}))^{5\times 4},$$

hence there is a constant $C(\hat{\mathcal{K}})$, such that for all $\mathcal{F} \in (W^{2,q}(\hat{\mathcal{K}}))^{5\times 4}$, we have the inequality:

$$|E_\mathcal{K}(W_h, \mathcal{F})| \leq C(\hat{\mathcal{K}}) \parallel E_\mathcal{K} \parallel^*_{2,q,\hat{\mathcal{K}}} [\mathcal{F}]_{2,q,\hat{\mathcal{K}}}$$

with:

$$\parallel E_\mathcal{K} \parallel^*_{2,q,\hat{\mathcal{K}}} := \sup_{0 \neq \mathcal{F} \in (W^{2,q}(\hat{\mathcal{K}}))^{5\times 4}} \frac{|E_\mathcal{K}(W_h, \mathcal{F})|}{\parallel \mathcal{F} \parallel_{2,q,\hat{\mathcal{K}}}} \leq C h_\mathcal{T}^4 \parallel W_h \parallel_{1,\infty,\mathcal{K}} .$$

Using the following inequalities (29)-(31), which are also valid with $\hat{\mathcal{S}}_m$ replaced with $\hat{\mathcal{K}}$ and $\mathcal{S}_m$ with $\mathcal{K}$, we obtain the following estimate:

$$|E_\mathcal{K}(W_h, \mathcal{F})| \leq C h_\mathcal{T}^{6-4/q} |\mathcal{F}|_{2,q,\mathcal{K}_j^n} \parallel W_h \parallel_{1,\infty,\mathcal{K}} . \tag{37}$$

The estimate (36) then results from the fact that the W_h are chosen from the finite dimensional space $V_h^1(\mathcal{T}_h^n)$ in which all norms are equivalent. □

We can also approximate (19) with a three point product Gauss quadrature rule and define the quadrature error functional $E^G_{\mathcal{K}}$ for the integration of the element volume fluxes in the same way as $E_{\mathcal{K}}$ in (35) with the Taylor quadrature rule replaced with the product Gauss quadrature rule.

An upper bound for the quadrature error of the volume flux integrals using the three point product Gauss quadrature rule is provided by the following lemma:

Lemma 7 *Let the tessellation $\mathcal{T}^n_h$ be as in Lemma 4. Let $\mathcal{F} \in \left(W^{s,q}_B(\mathcal{T}^n_h)\right)^{5\times 4}$, with $s, q \in \mathbb{R}$, $1 \leq q < \infty$, $sq > 4$, $(s-2)q \geq 1$, s integer when $q = 1$, and $W_h \in V^1_h(\mathcal{T}^1_h)$, then the quadrature error $|E^G_{\mathcal{K}}|$ can be estimated for all $\mathcal{K} \in \mathcal{T}^n_h$ as:*

$$|E^G_{\mathcal{K}}(W_h, \mathcal{F})| \leq C h^{6-4/q}_{\mathcal{T}} |\mathcal{F}|_{2,q,\mathcal{K}^n_j} \parallel W_h \parallel_{1,p,\mathcal{K}}, \tag{38}$$

with $\frac{1}{p} + \frac{1}{q} = 1$, and C a constant independent of h_k, $\mathcal{F}$ and W_h.

Proof. The three point product Gauss quadrature rule is exact if $\hat{W}_h \in (Q_1(\hat{\mathcal{S}}))^5$ and $\mathcal{F} \in (Q_1(\hat{\mathcal{S}}))^{5\times 4}$ and we can apply the Bramble-Hilbert lemma in the same way as for Lemma 6. The remaining part of the proof is nearly identical to Lemma 6 and is not repeated here. □

5.4 Truncation error of space-time discontinuous Galerkin discretization

The effect of the quadrature rule on the accuracy of the discontinous Galerkin discretization can be investigated by analyzing the truncation error. If we integrate (7) by parts, and introduce the numerical discretization operator $L_h : V_h(\mathcal{T}^n_h) \rightarrow V^1_h(\mathcal{T}^n_h)$, then we can write the weak formulation for the DG discretization as:

Find an $\mathcal{F}_h \in V^1_h(\mathcal{T}^n_h)$, such that for all $W_h \in V^1_h(\mathcal{T}^n_h)$:

$$\left(L_h(\mathcal{F}_h), W_h\right)_{\mathcal{E}_h} = 0,$$

with $\mathcal{E}_h = \cup_{n=0}^{N_T} \cup_{j=1}^{N_n} \mathcal{K}^n_j$ and:

$$(U, V)_{\mathcal{E}_h} = \sum_{n=0}^{N_T} \sum_{j=1}^{N_n} \int_{\mathcal{K}^n_j} U \cdot V d\mathcal{K}, \qquad \forall U, V \in V_h(\mathcal{T}^n_h).$$

The operator $L_h(\mathcal{F}_h)$ therefore is an approximation to $\mathrm{div}\mathcal{F}$. We can state now the following proposition, which provides information about the truncation error of the numerical discretization, including the effect of the Taylor quadrature for the flux integrals.

Proposition 1 *Let the tessellation $\mathcal{T}^n_h$ be as in Lemma 4, with $h_{\mathcal{T}}$ the diameter of the smallest ball containing the elements $\mathcal{K} \in \mathcal{T}^n_h$, with $h_{\mathcal{T}} \leq 1$. Let $W_h \in V^1_h(\mathcal{T}^1_h)$ and $\mathcal{F} \in (W^{t,q}_B(\mathcal{T}^n_h))^{5\times 4}$ with*

$s, t, q \in \mathbb{R}$, $1 < q < \infty$, $(s-1)q > 4$, $(s-2)q \geq 1$, and $0 \leq s \leq t$, then the truncation error of the approximation to $\mathrm{div}\mathcal{F}$ *in each space-time element $\mathcal{K} \in \mathcal{T}_h^n$ is equal to:*

$$|||L_h(\mathcal{F}) - \mathrm{div}\mathcal{F}|||_{s,q,\mathcal{T}_h^n} \leq C_0 h_{\mathcal{T}}^{t-s} |||\mathcal{F}(U)|||_{t+1,q,\mathcal{T}_h^n} + C_1 h_{\mathcal{T}}^{6-4/q} \lfloor \mathcal{F}(U) \rfloor_{2,q,\mathcal{T}_h^n} + C_2 h_{\mathcal{T}}^{2-1/p} \big(|\lfloor \mathcal{F}^+(U) \rfloor|_{2,q,\mathcal{T}_h^n} + |\lfloor \mathcal{F}^-(U) \rfloor|_{2,q,\mathcal{T}_h^n} \big), \tag{39}$$

with $\frac{1}{p} + \frac{1}{q} = 1$, and C_i, $i = 0, \cdots, 2$, positive constants independent of $\mathcal{F}$ and $h_{\mathcal{T}}$. The constant C_2 depends on the grid velocity.

Proof. We split the truncation error in each element $\mathcal{K} \in \mathcal{T}_h^n$ into a contribution related to the interpolation error and a contribution related to the discontinous Galerkin discretization:

$$\| L_h(\mathcal{F}) - \mathrm{div}\mathcal{F} \|_{s,q,\mathcal{K}} \leq \| \mathrm{div}\mathcal{F} - \mathbb{P}_{V_h^1(\mathcal{T}_h^n)}(\mathrm{div}\mathcal{F}) \|_{s,q,\mathcal{K}} + \| L_h(\mathcal{F}) - \mathbb{P}_{V_h^1(\mathcal{T}_h^n)}(\mathrm{div}\mathcal{F}) \|_{s,q,\mathcal{K}} \tag{40}$$

$$= e_1 + e_2, \tag{41}$$

with $\mathbb{P}_{V_h^1(\mathcal{T}_h^n)}$ the projection onto the space $V_h^1(\mathcal{T}_h^n)$. The contributions e_1 and e_2 are provided by Lemmas 8 and 9. If we sum (41) over all elements $\mathcal{K} \in \mathcal{T}_h^n$ and use the Minkovski inequality then we obtain the estimate (39), with the norm and semi-norms in $W_B^{s,q}(\mathcal{T}_h^n)$ defined in Appendix A.□

Lemma 8 *Let the tessellation $\mathcal{T}_h^n$ be as in Lemma 4 and assume that each $\mathcal{K} \in \mathcal{T}_h^n$ is star shaped with respect to some ball. Suppose $s, t, q \in \mathbb{R}$ with $1 \leq q \leq \infty$ and either $(t-1)q > 4$ when $q > 1$ or $t \geq 5$ when $q = 1$. Then for all $\mathcal{F} \in (W^{t,q}(\mathcal{K}))^{5\times 4}$ and $0 \leq s \leq t$ we have:*

$$\| \mathrm{div}\mathcal{F} - \mathbb{P}_{V_h^1(\mathcal{T}_h^n)}(\mathrm{div}\mathcal{F}) \|_{s,q,\mathcal{K}} \leq C h_{\mathcal{T}}^{t-s} \| \mathcal{F} \|_{t+1,q,\mathcal{K}} . \tag{42}$$

Proof. For integer values of s and t this lemma is a direct consequence of Theorem 4.4.4 in Brenner and Scott (Ref. 8), because the condition $|J_{G_K^{-1}}| \leq C/h_{\mathcal{T}}^4$ also ensures that $\gamma_{\mathcal{K}} = h_{\mathcal{K}}/\rho_{\mathcal{K}} > 0$, with ρ_K the radius of the smallest sphere completely contained in $\mathcal{K}$. For non-integer values of s and t we use Banach space interpolation between the estimates for integer values of s and t. If we define the operator $Tv := v - \mathbb{P}_{V_h^1(\mathcal{T}_h^n)} v$ and use the Banach space interpolation theorem for linear operators (Prop. 12.1.5 in (Ref. 8)) then we obtain with $m = [t]$ and $i = [s]$ the estimate:

$$\| T \|_{[W^{m,p}(\mathcal{K}), W^{m+1,p}(\mathcal{K})]_{\theta,p} \to [W^{i,p}(\mathcal{K}), W^{i+1,p}(\mathcal{K})]_{\theta,p}} \leq C h_{\mathcal{T}}^{m-i},$$

with $0 < \theta < 1$. Using Theorem 12.2.3 in (Ref. 8), which states that $W^{m+\theta,p}(\mathcal{K}) = [W^{m,p}(\mathcal{K}), W^{m+1,p}(\mathcal{K})]_{\theta,p}$ if the domain $\mathcal{K}$ has a Lipschitz continuous boundary, we obtain the estimate (42) with $s = i + \theta$,

$t = m + \theta$ and $v = \mathrm{div}\mathcal{F}$. The Lipschitz condition on $\mathcal{K}$ is satisfied because $\hat{\mathcal{K}}$ is Lipschitz and the mapping G_K, used to define $\mathcal{K} \in \mathcal{T}_h^n$ from $\hat{\mathcal{K}}$, is a C^1 diffeomorphism. □

Lemma 9 *Let the tessellation $\mathcal{T}_h^n$, flux tensor $\mathcal{F}$, and test function W_h be as in Proposition 1, then for each $\mathcal{K} \in \mathcal{T}_h^n$ we have the estimate:*

$$\| L_h(\mathcal{F}) - \mathbb{P}_{V_h^1(\mathcal{T}_h^n)}(\mathrm{div}\mathcal{F}) \|_{s,q,\mathcal{K}} \leq C_1 h_{\mathcal{T}}^{6-4/q} |\mathcal{F}(U)|_{2,q,\mathcal{K}} + C_2 h_{\mathcal{T}}^{2-1/p} (|\mathcal{F}^+(U)|_{2,q,\partial\mathcal{K}} + |\mathcal{F}^-(U)|_{2,q,\partial\mathcal{K}})$$

with $\frac{1}{p} + \frac{1}{q} = 1$.

Proof. Define $E(W_h) = E_{\partial\mathcal{K}}(W_h) + E_{\mathcal{K}}(W_h)$ as the error functional, with $E_{\partial\mathcal{K}}$ and $E_{\mathcal{K}}$ defined in (27) and (35), respectively. To each $W_h \in (W^{m,q}(\mathcal{K}))^5$, with m integer, $\mathcal{K} \in \mathcal{T}_h^n$, we can associate the vector $P\,W_h := (D^\alpha W_h) \in (L_N^q(\mathcal{K}))^5$, (see Appendix A), by ordering the N multi-indices α, satisfying $|\alpha| \leq m$, in a convenient way. Let $1 \leq p < \infty$. The representation theorem for linear functions in the dual space of the Sobolev space $W^{m,p}(\mathcal{K})$ (Adams (Ref. 1), Theorem 3.8), states that there exists an element $v \in (L_N^q(\mathcal{K}))^5$, with $\frac{1}{p} + \frac{1}{q} = 1$, such that writing the vector v in the form $(v_\alpha)_{0\leq|\alpha|\leq m}^5$ we have for all $W_h \in (W^{m,p}(\mathcal{K}))^5$ the following representation for the error functional $E(W_h)$:

$$E(W_h) = \sum_{0\leq|\alpha|\leq m} \int_{\mathcal{K}} D^\alpha W_h \, v_\alpha \, d\hat{\mathcal{K}}. \tag{43}$$

Moreover,

$$\inf_{v\in\mathcal{B}} \| v \|_{(L_N^q(\mathcal{K}))^5} = \| E \|_{m,p,\mathcal{K}}^*, \tag{44}$$

with $\mathcal{B}$ the set of all $v \in (L_N^q(\mathcal{K}))^5$ for which (43) holds for every $W_h \in (W^{m,p}(\mathcal{K}))^5$. For $1 < p < \infty$ the element $v \in (L_N^q(\mathcal{K}))^5$ satisfying (43) and (44) is unique. If we integrate E by parts then we obtain the representation:

$$\begin{aligned} E(W_h) &= \int_{\mathcal{K}} W_h \cdot \big(L_h(\mathcal{F}) - \mathrm{div}\mathcal{F}\big) d\mathcal{K} \\ &= \int_{\mathcal{K}} W_h \cdot \big(L_h(\mathcal{F}) - \mathbb{P}_{V_h^1(\mathcal{T}_h^n)}(\mathrm{div}\mathcal{F})\big) d\mathcal{K}. \end{aligned}$$

Since $v \in (L_N^q(\mathcal{K}))^5$ is unique for $1 < p < \infty$, we must have the relation:

$$v = L_h(\mathcal{F}) - \mathbb{P}_{V_h^1(\mathcal{T}_h^n)}(\mathrm{div}\mathcal{F}). \tag{45}$$

Hence, the minimum is attained when v satisfies (45), and using (44) we have the relation:

$$\| L_h(\mathcal{F}) - \mathbb{P}_{V_h^1(\mathcal{T}_h^n)}(\mathrm{div}\mathcal{F}) \|_{(L_N^q(\mathcal{K}))^5} = \| E \|_{m,p,\mathcal{K}}^* . \tag{46}$$

The space $(W^{m,q}(\mathcal{K}))^5$ is a closed subspace W of $(L_N^q)^5$ and there exists an isometric isomorphism from $(W^{m,q}(\mathcal{K}))^5$ onto $W \subset (L_N^q(\mathcal{K}))^5$ (see Adams (Ref. 1), page 46). Since $L_h(\mathcal{F}) - \mathrm{div}\mathcal{F} \in (W^{m,q}(\mathcal{K}))^5$, because $\mathcal{F} \in (W_B^{t,q}(\mathcal{T}_h^n))^{5\times 4}$, we can therefore transform (46) into:

$$\| L_h(\mathcal{F}) - \mathbb{P}_{V_h^1(\mathcal{T}_h^n)}(\mathrm{div}\mathcal{F}) \|_{m,q,\mathcal{K}} = \| E \|^*_{m,p,\mathcal{K}} .$$

Using Banach space interpolation we can extend this relation also to noninteger values of m. For more details, see Lions (Ref. 13) and Adams (Ref. 1).

The proof is completed using the estimates provided by Lemmas 4 and 6 and the inequality $\| W_h \|_{1,p,\mathcal{K}} \leq \| W_h \|_{s,p,\mathcal{K}}$ for $s \geq 1$:

$$\begin{aligned}
&\| L_h(\mathcal{F}) - \mathbb{P}_{V_h^1(\mathcal{T}_h^n)}(\mathrm{div}\mathcal{F}) \|_{s,q,\mathcal{K}} \\
&\quad \leq \sup_{0\neq W_h \in \left(W^{s,p}(\mathcal{K})\right)^5} \frac{|E_{\mathcal{K}}(\nabla W_h, \mathcal{F})|}{\| W_h \|_{s,p,\mathcal{K}}} + \sup_{0\neq W_h \in \left(W^{s,p}(\mathcal{K})\right)^5} \tfrac{1}{2} \frac{|E_{\partial\mathcal{K}}(W_h^-, \mathcal{F}^+)|}{\| W_h \|_{s,p,\mathcal{K}}} + \\
&\qquad \sup_{0\neq W_h \in \left(W^{s,p}(\mathcal{K})\right)^5} \tfrac{1}{2} \frac{|E_{\partial\mathcal{K}}(W_h^-, \mathcal{F}^-)|}{\| W_h \|_{s,p,\mathcal{K}}} \\
&\quad \leq C_1 h_{\mathcal{T}}^{6-4/q} |\mathcal{F}(U)|_{2,q,\mathcal{K}} + C_2 h_{\mathcal{T}}^{2-1/p} \left(|\mathcal{F}^+(U)|_{2,q,\partial\mathcal{K}} + |\mathcal{F}^-(U)|_{2,q,\partial\mathcal{K}} \right) \qquad (47)
\end{aligned}$$

with $\frac{1}{p} + \frac{1}{q} = 1$. □

Remark 5 *For $q = 1/(1-\epsilon)$, $s > 5$ and $t \geq 7$ in Proposition 1, with $\epsilon \in \mathbb{R}^+$ an arbitrary positive number, the trunction error of the discontinuous Galerkin discretization, including the effect of the approximation of the element surface and volume integrals, is $O(h_{\mathcal{T}}^{2-\epsilon})$ in the $W_B^{s,q}(\mathcal{T}_h^n)$ norm. This shows that the Taylor quadrature rule does not negatively influence the second order accuracy of the numerical discretization, since we can choose ϵ arbitrary small.*

Corollary 1 *Let the conditions of Proposition 1 be satisfied, with $(s-1)q > 4$ replaced by $sq > 4$, then the product Gauss quadrature rules defined above Lemma 5 and Lemma 7 result in the same truncation error as obtained for the Taylor quadrature rule in Proposition 1.*

Proof. The proof is immediate if one uses the estimates provided by Lemmas 5 and 7 in (47).□

Remark 6 *The reader is referred to Part I for an experimental verification of the error. For a steady subsonic entropy preserving flow a global L^2-error of the order $h_{\mathcal{T}}^{2.5}$ was found from numerical experiments, using data at superconvergence points, even on locally refined meshes.*

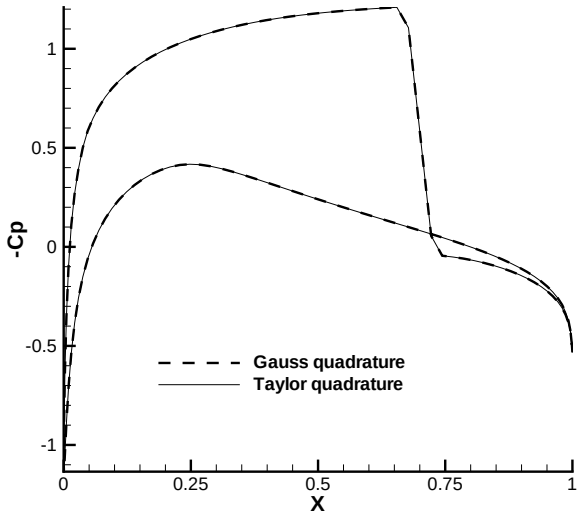

Fig. 1 Comparison of pressure distribution for the transonic over a NACA0012 foil.

6 Results

6.1 NACA0012

A first comparison of the two point product Gauss quadrature rule and the Taylor quadrature rule is presented in Figure 1. Transonic flow over a NACA0012 airfoil has been simulated with a freestream Mach number of 0.8, and an angle of attack of 2 degrees. Both the Taylor quadrature rule and the product Gauss quadrature rule of Corollary 1 have been used. In this and the following experiments the system of equations is solved as described in Part I. Clearly, the results in Figure 1 show hardly any difference in the pressure distribution over the airfoil. The lift coefficient are computed to be 0.5387 for the Taylor quadrature rule, and 0.5348 for the Gauss quadrature rule. The small increase in lift is most probably caused by the fact that the Taylor quadrature rule is slightly less dissipative.

6.2 Cylinder flow

In an interesting article, Bassi and Rebay (Ref. 3) found that the second order DG method using first order polynomials for both the flow representation and the geometry elements produced a severe numerical boundary layer for the inviscid subsonic flow past a cylinder. Bassi et al. apply the standard steady-state RKDG algorithm of Cockburn et al. (Ref. 10), but without the use of a limiter, since the flow is subsonic. In their simulations they used an exact Riemann solver, the

equations were discretized on a triangular mesh, and a Gauss quadrature rule was used to evaluate the flux integrals.

The numerical experiment of Bassi and Rebay has been repeated. Subsonic flow past a cylinder has been simulated at a Mach number $M_\infty = 0.38$, on a fine 64×96 mesh and a coarse 32×48 mesh, both with rectangular elements, which are described using the bilinear isoparametric map. On the coarse mesh also a quadratic superparametric representation of the boundary has been used. Both the Gauss and Taylor quadrature rule have been applied. No artifical dissipation has been added, and all simulations have been converged to machine accuracy. The numerical boundary layers are presented in Figure 2; the numerical boundary layer is represented by the total pressure loss, defined as

$$p_{t-loss} = 1 - \frac{p}{p_\infty} \left(\frac{1 + \frac{1}{2}(\gamma - 1)M^2}{1 + \frac{1}{2}(\gamma - 1)M_\infty^2} \right)^{\frac{\gamma}{\gamma - 1}},$$

where M is the local Mach number, and γ is the ratio of specific heats. Clearly, the Taylor quadrature rule results in a significant reduction of the numerical boundary layer. This difference can be attributed to the fact that in the Gauss quadrature rule the normal flux is computed at different locations in the element face. At each quadrature point we consider a one-dimensional Riemann problem and neglect the tangential variation of the solution in the element face. The tangential vectors at the quadrature points are slightly different and this results in different shear wave contributions from the quadrature points, which manifest themselves in spurious entropy generation near the wall. The Taylor quadrature rule considers the Riemann problem only at one point and therefore results in a more consistent discretization when combined with one-dimensional (approximate) Riemann solvers.

Bassi and Rebay reported that it was mandatory to use higher order boundary representation in order to get correct results. In particular, their numerical boundary was found *not* to dissappear under grid refinement. This may have been caused by the fact that their computation failed to converge on the finer meshes. Though they do not present a total pressure loss distribution for linear boundary elements, the strength of the numerical wake shown in the Mach field plots, would imply a total pressure loss far exceeding 10%, which is more than experienced in our simulations. As shown in Figure 2, a superparametric boundary representation does improve the flow results, but since the numerical boundary layer on the coarse mesh is not all that bad, the improvement is not as dramatic as with Bassi and Rebay.

Actually, the accuracy improvement under grid refinement, uniform or local, is greater than when using superparametric elements. This is already clear from Figure 2 where the fine grid results are

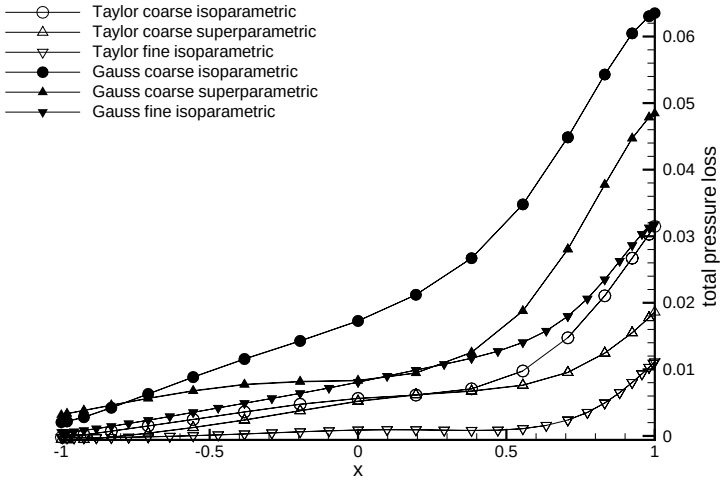

Fig. 2 Comparison of the total pressure loss at the wall for the flow around a circular cylinder ($M_\infty = 0.38$) using Gauss and Taylor flux quadrature rules for isoparametric elements on a coarse (32×48 elements) and fine mesh (64×96 elements) and superparametric elements on a coarse mesh (32×48 elements).

more accurate than the coarse superparametric results. The grid refinement efficiency is demonstrated more strongly in Figure 3, where the previous results are compared with results obtained under local grid refinement. The coarse mesh has been refined three times and the Mach number distributions are shown. The adapted meshes are obtained through local grid refinement near the cylinder, and at each adaptation the number of boundary cells in the circumferential direction is doubled. Accuracy on the one time refined mesh is comparable to the fine mesh computation, and the numerical boundary layer all but disappears on the three times refined mesh (maximum total pressure loss of 0.2 percent). Hence it is not necessary to use a higher-order accurate boundary representation in order to obtain accurate simulation results. More details can be found in Van der Vegt et al. (Ref. 21).

6.3 Lambda shock

In order to demonstrate the shock-capturing capabilities of the present DG method, transonic flow around the ONERA M6 wing has been simulated with a Mach number of 0.84 and an angle of attack of 3.06 degrees. The grid consists of 440,000 cells. The pressure distribution on the wing and at the symmetry plane is shown in Figure 4, the lambda shock structure is clearly visible. In Figure 5 the pressure distribution at the cross sections at 65% span and at 90% span are compared with experiment. Considering the fact that in the simulations the flow is considered to be inviscid,

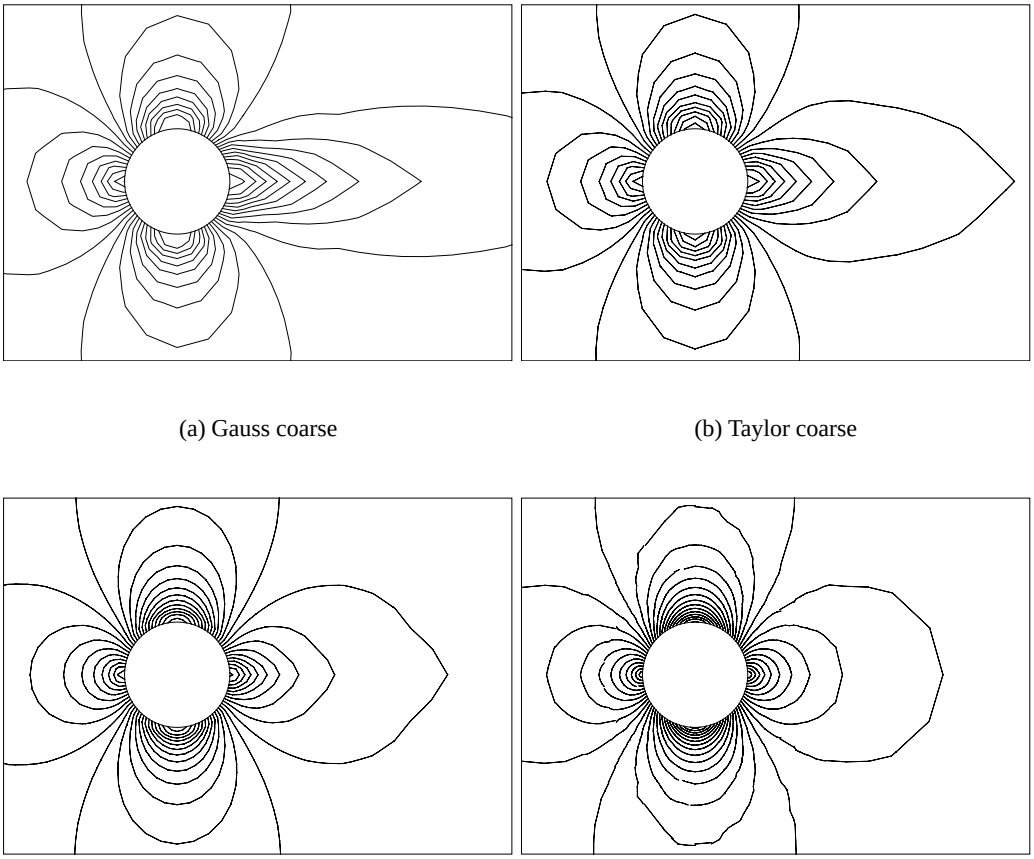

(a) Gauss coarse

(b) Taylor coarse

(c) Taylor fine

(d) Taylor three adaptations

Fig. 3 Comparison of the Mach number field of a circular cylinder at $M_\infty = 0.38$ using Gauss and Taylor quadrature with (locally refined) linear isoparametric elements (coarse mesh with 1536 cells, fine mesh with 6144 cells, and three times adapted coarse mesh with 8358 elements).

agreement is good.

6.4 Computational efficiency

Steady, subsonic flow over an ONERA M6 wing is simulated with a freestream Mach number of 0.4 and an angle of attack of six degrees. Even though the flow is stationary, it has been simulated with the space-time discretization. This example is chosen to measure the computational efficiency of the Taylor quadrature rule. Not only the quadrature rules are compared but also the numerical flux. The original version of the flow solver applied the Osher approximate Riemann solver. As explained above, for the development of the Taylor quadrature rule it proved necessary to change to

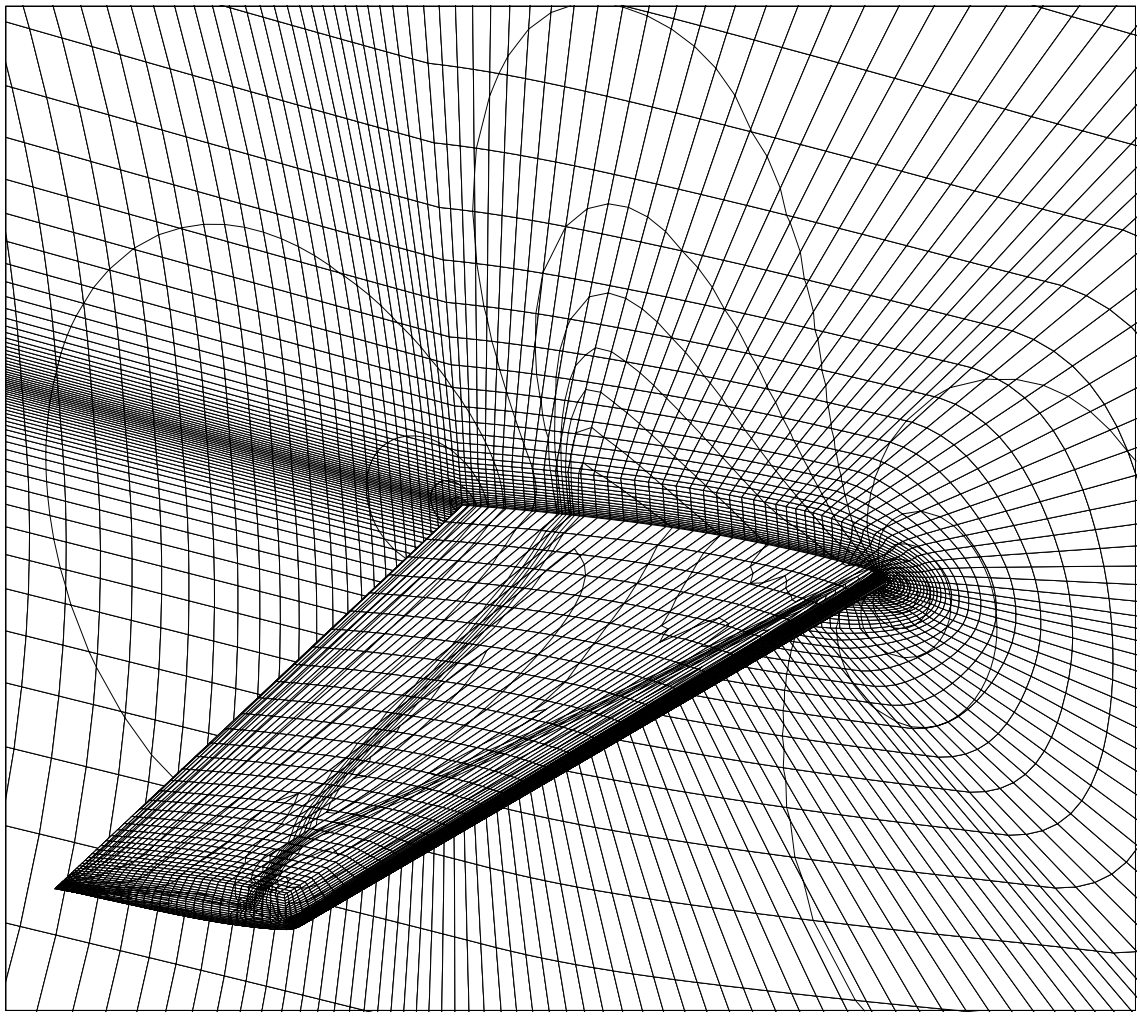

Fig. 4 Pressure distribution on wing and symmetry plane for the ONERA M6 wing.

the HLLC approximate Riemann solver. In Table 1 computing times and speeds for the complete execution of the flow solver are compared for three of the four combinations of quadrature rule and Riemann solver. Computing times are on a single processor NEC SX-5, for 100 multigrid cycles with one pre- and postrelaxation on a coarse mesh with 55,000 grid cells. In the transition from the Gauss quadrature rule combined with the Osher scheme to the Taylor quadrature rule combined with the HLLC scheme a speedup of six has been obtained. This is partly due to the reduced number of computations, and partly due to the data locality, which allows higher computational speeds.

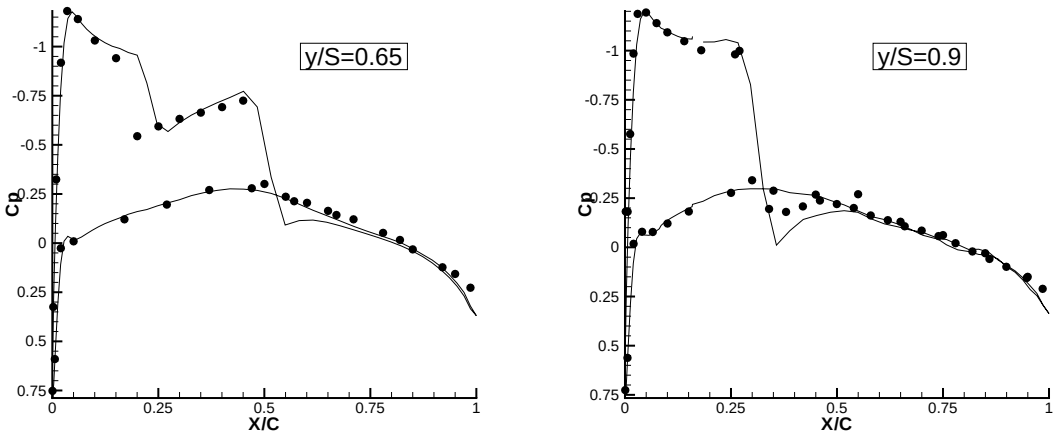

Fig. 5 Pressure distributions at 65% and 90% span for the ONERA M6 wing. Experimental results are shown with dots.

Table 1 Performance comparison of the different methods.

method	computing time [s]	speed [Gflop/s]
Osher scheme with Gauss quadrature	1628	2.2
HLLC scheme with Gauss quadrature	754	2.9
HLLC scheme with Taylor quadrature	274	3.4

6.5 First torsion mode of the AGARD 445.6 wing

Transonic flow at a freestream Mach number of 0.96 is simulated over the deforming AGARD 445.6 wing. The geometry deformation corresponds to the first torsion mode of the wing. The grid point displacements are only in the z-direction, and the average displacement is zero. Views of the normally flat wing at the two extreme positions are shown in Figure 6. Maximum displacement occurs at the tip and is of the order of 10% root chord. The normalized frequency of the torsion mode is 0.192, normalized with L/a_∞, where L is the root chord and a_∞ is the freestream speed of sound.

The wing deformations are accomodated by the grid using a standard grid deformation algorithm to move the grid points. The deformation algorithm essentially solves a Laplace equation for the grid point displacements (see Masud and Hughes (Ref. 15)).

The grid contains 73,728 grid points. The time period is subdivided into 20 uniform time steps, which are chosen such that the movement of the shock is captured accurately. Per time step the L_2-

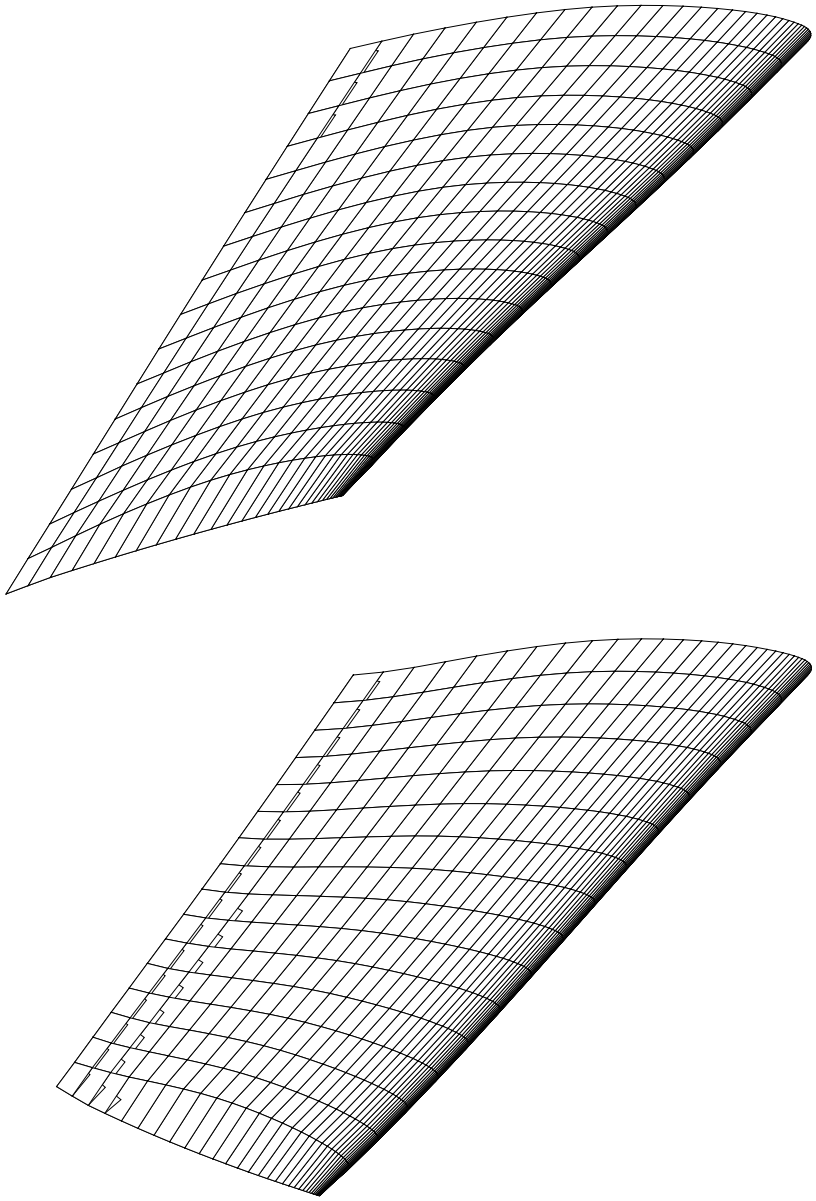

Fig. 6 Wing deformation at the two extreme positions. The vertical coordinate is multiplied with a factor 5, to make the deformation visible. The flow comes from the right.

residual for the cell averages is reduced to the level of 10^{-5}, which required 150 multigrid cycles on average. Part of the convergence histories are shown in Figure 7. Including postprocessing, the simulation of a period required 15,000 seconds on a single processor NEC SX-5 at a speed of 3.5 Gflop/s.

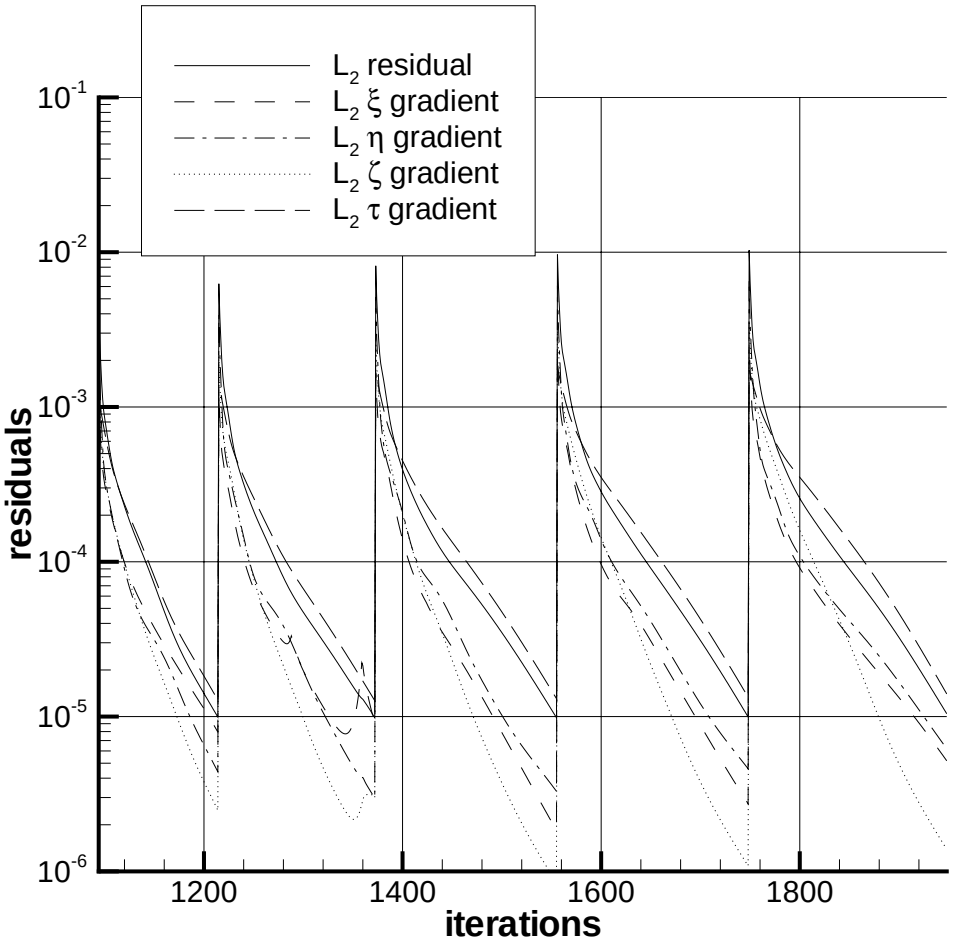

Fig. 7 Convergence history for five time steps of the simulation of the first torsion mode of the AGARD 445.6 wing

The Mach number distribution on the upper side of the wing and in the symmetry plane at $t = \frac{7}{20}$, where T is the period of the torsion mode, is shown in Figure 8. The pressure coefficient C_p at 88% span is shown in Figure 9. Also shown is the shape of the cross section geometry. The pressure coefficient shows strong variations during the oscillation cycle and a rapidly moving and oscillating shock is captured without numerical oscillations.

The results clearly demonstrate the matureness of the discontinuous Galerkin method. Efficient simulation of the three-dimensional unsteady flow over a deforming wing is possible using the space-time discontinuous Galerkin finite element method described in this article.

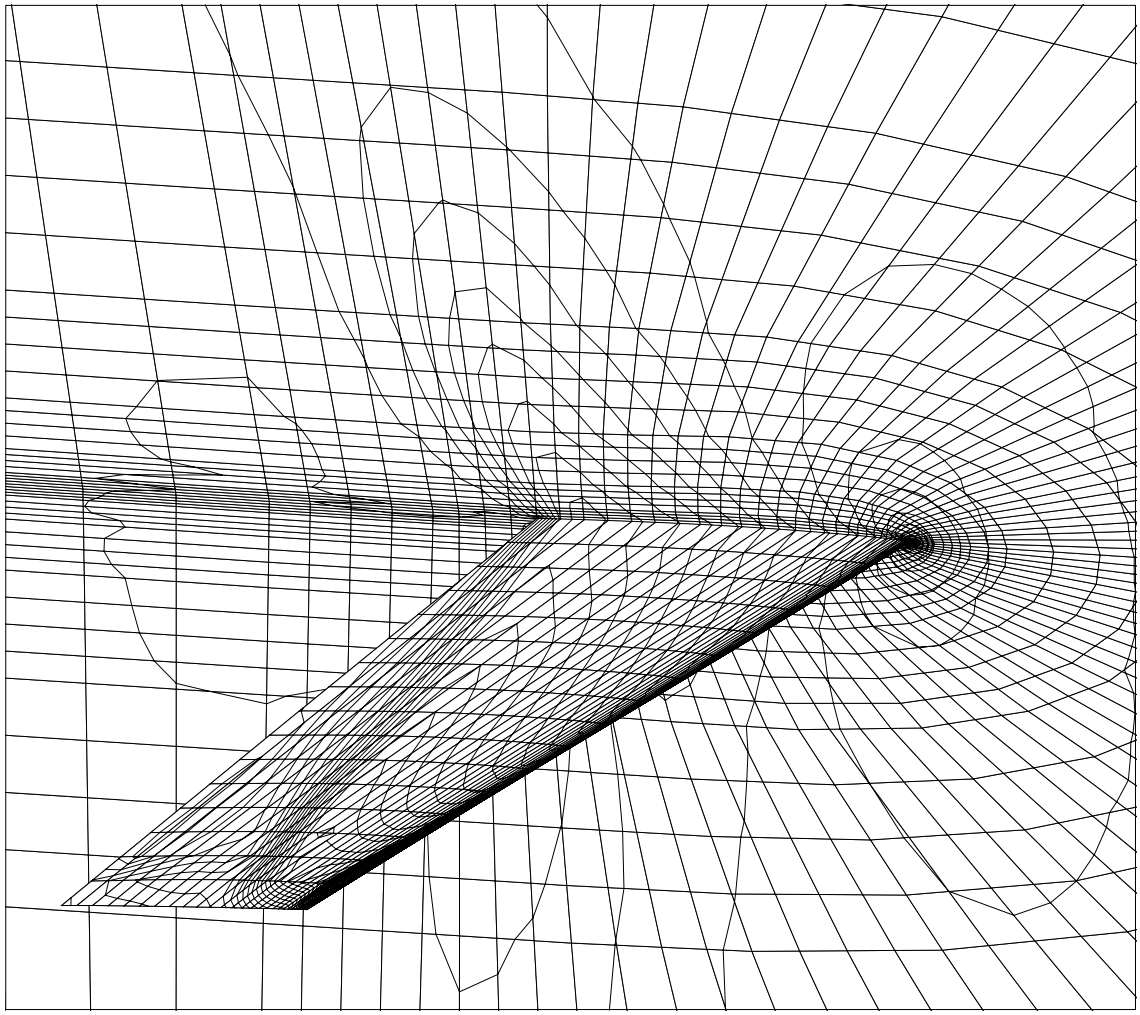

Fig. 8 Mach number contours on wing and symmetry plane at time $t = \frac{7}{20}T$, where T is the period of the torsion mode.

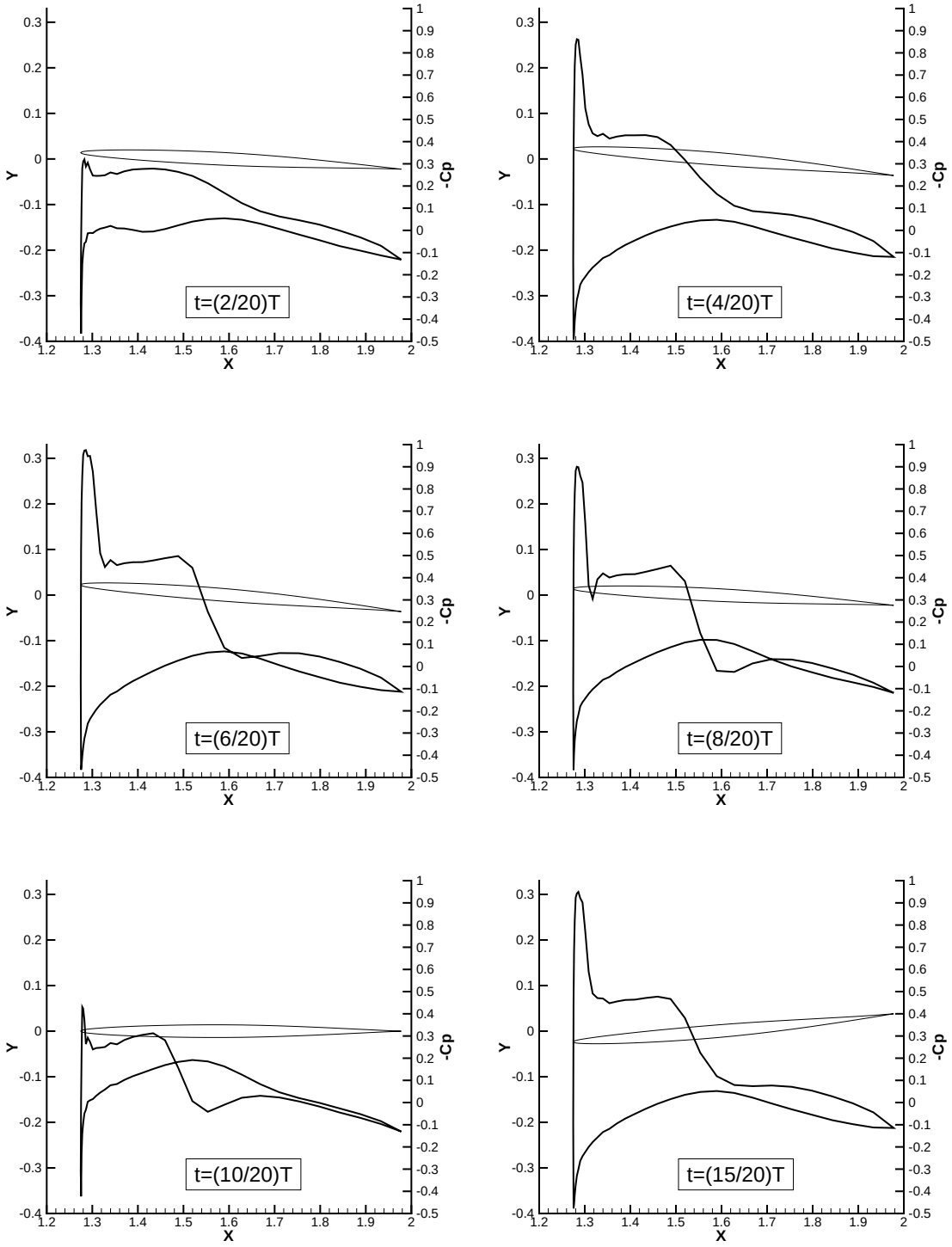

Fig. 9 C_p-distributions at a cross section at 88% span

7 Conclusions

In this article a new quadrature rule for the face flux integrals arising in the discontinuous Galerkin discretization of the Euler equations is presented. Basically, the quadrature rule expands the flux terms in a Taylor series in the face center. The key idea is that the gradient expansion coefficients are readily available in the DG method. This makes the Taylor quadrature rule very natural and highly efficient within the DG framework. A speedup of three has been obtained when comparing the computing times for Taylor quadrature rule with the computing times for the standard Gauss quadrature rule. Moreover, this gain in efficiency comes without any loss in accuracy. Namely, when combined with linear basis functions in the DG method, the new Taylor quadrature rule yields a second order local truncation error, just as the conventional Gauss quadrature rule does.

Numerical experiments have demonstrated the stability and accuracy of the method. The DG scheme combined with the Taylor quadrature rule is slightly less dissipative than the DG scheme combined with the Gauss quadrature rule. This emphasizes the importance of the particular face flux quadrature in discontinuous Galerkin methods. Clearly, more research has to be performed to completely understand the dissipative behaviour of the DG method, especially near slip walls.

The space-time discontinuous Galerkin discretization of the Euler equations combined with the Taylor quadrature rule has successfully been applied to the simulation of transonic flow over a deforming wing. Application of the method to helicopter rotor flows are presented elsewhere (Boelens et al. (Ref. 6)). These applications demonstrate the matureness of the discontinuous Galerkin method.

Acknowledgements

The advice and continued support by Dr. B. Oskam (NLR) during the course of this project is greatly appreciated. Sincere thanks are also due to O.J. Boelens (NLR) for conducting many simulations with the program HEXADAP which significantly contributed to the validation and improvements of the numerical scheme.

1. R.A. Adams. *Sobolev spaces.* Academic Press, 1975.
2. H.L. Atkins and C.W. Shu. Quadrature-free implementation of discontinuous Galerkin method for hyperbolic equations. *AIAA Journal*, 36(5):775–782, 1997.
3. F. Bassi and S. Rebay. High-order accurate discontinuous finite element solution of the 2D Euler equations. *J. Comput. Phys.*, 138:251–285, 1997.
4. P. Batten, N. Clarke, C. Lambert, and D.M. Causon. On the choice of wave speeds for the HLLC Riemann solver. *SIAM J. Sci. and Stat. Comp.*, 18(6), 1997.
5. P. Batten, M.A. Leschziner, and U.C. Goldberg. Average-state Jacobians and implicit methods for compressible viscous and turbulent flows. *J. Comput. Phys.*, 137:38–78, 1997.
6. O.J. Boelens, H. van der Ven, B. Oskam, and A.A. Hassan. The boundary conforming discontinuous Galerkin finite element approach for rotorcraft simulations. *submitted to J. of Aircraft*, 2001.
7. J.H. Bramble and S.R. Hilbert. Bounds for a class of linear functionals with applications to Hermite interpolation. *Numer. Math.*, 16:362–369, 1971.
8. S.C. Brenner and L.R. Scott. *The mathematical theory of finite element methods.* Springer Verlag, 1996.
9. P.G. Ciarlet. *The finite element method for elliptic problems.* North-Holland, 1978.
10. B. Cockburn, S. Hou, and C-W. Shu. The Runge-Kutta local projection discontinuous galerkin finite element method for conservation laws IV: the multidimensional case. *Math. Comp.*, 54:545–581, 1990.
11. B. Cockburn, G. Karniadakis, and C.-W. Shu, editors. *Discontinuous Galerkin Methods: Theory, Computation and Applications*, volume 11 of *Lecture Notes in Computational Science and Engineering.* Springer Verlag, Berlin, May 24-26 1999.
12. P. Grisvard. *Elliptic problems in nonsmooth domains.* Pitman, 1985.
13. J.-L. Lions. Sur les espaces d'interpolation; dualité. *Math. Scand.*, 9:147–177, 1961.
14. D.P. Lockard and H.L. Atkins. Efficient implementations of the quadrature-free discontinuous galerkin method. *AIAA Journal*, 99-3309, 1999.
15. A. Masud and T.J.R. Hughes. A space-time Galerkin/least squares finite element formulation of the Navier-Stokes equations for moving domain problems. *Comput. Meth. Appl. Mech. Engrg.*, 146:91–126, 1997.

16. S.M. Nikol'skii. On imbedding, continuation and approximation theorems for differentiable functions of several variables. *Russian Mat. Surveys*, 16:55–104, 1961.
17. E.F. Toro. *Riemann solvers and numerical methods for fluid dynamics.* Springer Verlag, Berlin, 1997.
18. H. Triebel. *Interpolation theory, function spaces, differential operators*. North-Holland, 1978.
19. J.J.W. van der Vegt. Geometric conditions on the invertibility and interpolation error of isoparametric hexahedral space-time elements. *submitted to Math. Comp.*, 2001.
20. J.J.W. van der Vegt and H. van der Ven. Discontinuous Galerkin finite element method with anisotropic local grid refinement for inviscid compressible flows. *J. Comput. Phys.*, 141:46–77, 1998.
21. J.J.W. van der Vegt and H. van der Ven. Slip boundary conditions in discontinuous Galerkin discretizations of the Euler equations of gas dynamics. In *Proceedings Fifth World Congress on Computational Mechanics*, `http://wccm.tuwien.ac.at/`, July 7-12, Vienna 2002.
22. J.J.W. van der Vegt and H. van der Ven. Space-time discontinuous Galerkin finite element method with dynamic grid motion for inviscid compressible flows. Part I. General formulation. *to appear in J. Comput. Phys.*, 2002.
23. H. van der Ven and J.J.W. van der Vegt. Accuracy, resolution, and computational complexity of a discontinuous Galerkin finite element method. In *(Ref. 11)*, pages 439–444, 2000.

This page is intentionally left blank.

Appendices

A Sobolev spaces

- A domain Ω has the cone property if there exists a finite cone C such that each point $x \in \Omega$ is the vertex of a finite cone C_x contained in Ω, which is obtained by rigid motion from C and is congruent to C, Adams (Ref. 1).
- Define the standard Sobolev space $W^{m,p}(\Omega)$, with $m \in \mathbb{Z}$, $m \geq 0$, $1 \leq p \leq \infty$, and $\Omega \subseteq \mathbb{R}^n$, as:

$$W^{m,p}(\Omega) := \left\{ v \in L^1_{loc}(\Omega) \;\middle|\; \| v \|_{m,p,\Omega} < \infty \right\}.$$

  Here $L^1_{loc}(\Omega)$ denotes the space of locally integrable functions:

$$L^1_{loc}(\Omega) := \left\{ v \,|\, v \in L^1(K), \;\; \forall \text{compact } K \subset \text{interior}\, \Omega \right\},$$

  and $L^1(K)$ the space of Lebesgue integrable functions on K. The Sobolev norm $\| v \|_{m,p,\Omega}$ is defined as:

$$\| v \|_{m,p,\Omega} := \Big(\sum_{|\alpha| \leq m} \int_\Omega |D^\alpha v|^p dx \Big)^{1/p}, \qquad \text{if } 1 \leq p < \infty,$$

$$\| v \|_{m,p,\Omega} := \max_{|\alpha| \leq m} \Big(\operatorname*{ess\,sup}_{x \in \Omega} |D^\alpha v(x)| \Big), \qquad \text{if } p = \infty,$$

  and the semi-norms $|v|_{m,p,\Omega}$ and $[v]_{m,p,\Omega}$ are for $1 \leq p < \infty$ defined as:

$$|v|_{m,p,\Omega} := \Big(\sum_{|\alpha| = m} \int_\Omega |D^\alpha v|^p dx \Big)^{1/p},$$

$$[v]_{m,p,\Omega} := \Big(\sum_{k=0}^{n} \int_\Omega \Big| \frac{\partial^m v}{\partial x_k^m} \Big|^p dx \Big)^{1/p},$$

  with α the multi-index symbol, and the usual modification for $p = \infty$. The derivatives in the (semi)-norms have to be considered as weak derivatives.
- For a bounded or unbounded open domain $\Omega \subseteq \mathbb{R}^n$ with the cone property the Sobolev space $W^{s,p}(\Omega)$, with $s \in \mathbb{R}$, $s \geq 0$, $1 \leq p \leq \infty$, is defined as: $W^{s,p}(\Omega) = W^{m,p}(\Omega)$ when $s = m$ is a non-negative integer, and for noninteger s as the subspace of $W^{m,p}(\Omega)$ with a finite Sobolev-Slobodečkij norm:

$$\| v \|_{s,p,\Omega} := \Big(\| v \|^p_{m,p,\Omega} + \sum_{|\alpha| = m} \int_\Omega \int_\Omega \frac{|D^\alpha v(x) - D^\alpha v(y)|^p}{|x - y|^{m + \sigma p}} dx\, dy \Big)^{1/p}, \quad 1 \leq p < \infty$$

$$\| v \|_{s,p,\Omega} := \max \Big(\| v \|_{m,\infty,\Omega}, \max_{|\alpha| = m} \operatorname*{ess\,sup}_{x,y \in \Omega, x \neq y} \frac{|D^\alpha v(x) - D^\alpha v(y)|}{|x - y|^\sigma} \Big), \qquad p = \infty,$$

with m the integer part of s, and $\sigma = s - m$, with $0 < \sigma < 1$. Note, with this definition fractional order Sobolev spaces coincide for s noninteger and $1 < p < \infty$ with the Besov spaces defined in Triebel (Ref. 18), pages 310 and 323 (see also (Ref. 16)), for which extensive imbedding theorems exist.

- Define the broken Sobolev space $W_B^{s,p}(\mathcal{T}_h^n)$, with $s \in \mathbb{R}$, $s \geq 0$ and $1 \leq p \leq \infty$, as:

$$W_B^{s,p}(\mathcal{T}_h^n) := \left\{ v \in L^p(\mathcal{T}_h^n) \;\middle|\; v|_{\mathcal{K}} \in W^{s,p}(\mathcal{K}_j^n),\ \forall \mathcal{K}_j^n \in \mathcal{T}_h^n \right\}, \tag{48}$$

with the norm and semi-norms defined as:

$$\begin{aligned} |||v|||_{s,p,\mathcal{T}_h^n} &= \Big(\sum_{\mathcal{K} \in \mathcal{T}_h^n} \| v \|_{s,p,\mathcal{K}}^p \Big)^{1/p} \\ \lfloor v \rfloor_{s,p,\mathcal{T}_h^n} &= \Big(\sum_{\mathcal{K} \in \mathcal{T}_h^n} |v|_{s,p,\mathcal{K}}^p \Big)^{1/p} \\ |\lfloor v \rfloor|_{s,p,\mathcal{T}_h^n} &= \Big(\sum_{\mathcal{K} \in \mathcal{T}_h^n} |v|_{s,p,\partial\mathcal{K}}^p \Big)^{1/p}. \end{aligned}$$

- The norms and semi-norms on product spaces are extended naturally. For instance if $v \in \mathbb{R}^n$, $v = (v_1, \cdots, v_n)$ then:

$$\| v \|_{m,p,\Omega} = \Big(\sum_{i=1}^{n} \| v_i \|_{m,p,\Omega}^p \Big)^{1/p}, \qquad \text{if } 1 \leq p < \infty, \tag{49}$$

$$\| v \|_{m,\infty,\Omega} = \max_{1 \leq i \leq n} \| v_i \|_{m,\infty,\Omega}, \tag{50}$$

$$|[v]|_{m,\infty,\Omega} = \max_{1 \leq i \leq n} \sup_{x \in \Omega} \left\| \frac{\partial^m v(x)}{\partial x_i^m} \right\|, \tag{51}$$

with $\| \cdot \|$ the Euclidian norm.

- The product space L_N^p is defined for $1 \leq p < \infty$ as:

$$L_N^p(\Omega) = \Pi_{j=1}^N L^p(\Omega),$$

with the associated norm given by (49).

B Some facts from differential geometry

Given a parametrization $F : (-1,1)^{n-1} \to S$, where S is curved hypersurface in $\mathbb{R}^n$, integration over the surface S is defined as:

$$\int_S f(x)dx = \int_{(-1,1)^{n-1}} f(F(\xi)) \left| \frac{\partial F}{\partial \xi_1} \wedge \cdots \wedge \frac{\partial F}{\partial \xi_{n-1}} \right| d\xi,$$

where the outer product $v = w_1 \wedge \cdots \wedge w_{n-1}$, for $n-1$ vectors w_i in $\mathbb{R}^n$, is defined component-wise by the rule

$$v^j = \det(w_1, \ldots, w_{n-1}, e_j),$$

with e_j the j-th basis vector in $\mathbb{R}^n$. From this formula it is clear that this concept is a generalization of the outer product in $\mathbb{R}^3$.

Let $\mathcal{S}_m$ ($1 \leq m \leq 6$) be one of the six space-time faces of the element $\mathcal{K}$ which is parametrized by the map G_K. Let $F_{\mathcal{S}_m}$ be the parametrization of $\mathcal{S}_m$ obtained from the restriction of G_K to the appropriate face of the boundary of $\hat{\mathcal{K}} = (-1,1)^4$. As computed in Part I we have:

$$\frac{\partial F_{\mathcal{S}_m}}{\partial \xi_{m_2}} \wedge \frac{\partial F_{\mathcal{S}_m}}{\partial \xi_{m_3}} \wedge \frac{\partial F_{\mathcal{S}_m}}{\partial \xi_4} = \begin{pmatrix} \frac{1}{2}\Delta t \frac{\partial F_{S_m(t)}}{\partial \xi_{m_2}} \wedge \frac{\partial F_{S_m(t)}}{\partial \xi_{m_3}} \\ -\frac{1}{2}\Delta \overline{x} \cdot \left(\frac{\partial F_{S_m(t)}}{\partial \xi_{m_2}} \wedge \frac{\partial F_{S_m(t)}}{\partial \xi_{m_3}} \right) \end{pmatrix}, \tag{52}$$

where the outer product on the right hand side is the usual outer product in $\mathbb{R}^3$ and $\Delta \overline{x} = F_K^{n+1}(\bar{\xi}) - F_K^n(\bar{\xi})$. The parametrization $F_{S_m(t)}$ of the space face $S_m(t)$ at time t is obtained by a further restriction of $F_{\mathcal{S}}$ to a constant computational time coordinate. Note that $\frac{\partial F_{S_m(t)}}{\partial \xi_{m_2}} \wedge \frac{\partial F_{S_m(t)}}{\partial \xi_{m_3}}$ is aligned with the space normal of $S_m(t) \subset \partial K(t) \subset \mathbb{R}^3$. By construction the outer product is aligned with the space-time normal n of $\mathcal{S}_m$:

$$n = s \frac{\frac{\partial F_{\mathcal{S}}}{\partial \xi_{m_2}} \wedge \frac{\partial F_{\mathcal{S}}}{\partial \xi_{m_3}} \wedge \frac{\partial F_{\mathcal{S}}}{\partial \xi_4}}{\left| \frac{\partial F_{\mathcal{S}}}{\partial \xi_{m_2}} \wedge \frac{\partial F_{\mathcal{S}}}{\partial \xi_{m_3}} \wedge \frac{\partial F_{\mathcal{S}}}{\partial \xi_4} \right|},$$

where $s = \pm 1$ is such that the normal is outward pointing. By definition,

$$\int_{\mathcal{S}_m} f n dx = s \int_{\hat{\mathcal{S}}} f \frac{\partial F_{\mathcal{S}_m}}{\partial \xi_{m_2}} \wedge \frac{\partial F_{\mathcal{S}_m}}{\partial \xi_{m_3}} \wedge \frac{\partial F_{\mathcal{S}_m}}{\partial \xi_4} d\xi_{m_2} d\xi_{m_3} d\xi_4, \tag{53}$$

hence the $\mathbb{R}^4$-valued measure $d\hat{\mathcal{S}}^m$, $1 \leq m \leq 6$, is defined as

$$d\hat{\mathcal{S}}^m = s \frac{\partial F_{\mathcal{S}_m}}{\partial \xi_{m_2}} \wedge \frac{\partial F_{\mathcal{S}_m}}{\partial \xi_{m_3}} \wedge \frac{\partial F_{\mathcal{S}_m}}{\partial \xi_4} d\xi_{m_2} d\xi_{m_3} d\xi_4.$$

Define the $\mathbb{R}^3$-valued measure $d\overline{\mathcal{S}}^m$ on $\hat{\mathcal{S}}$ by

$$d\overline{\mathcal{S}}^m = s \frac{\partial F_{S_m(t)}}{\partial \xi_{m_2}} \wedge \frac{\partial F_{S_m(t)}}{\partial \xi_{m_3}} d\xi_{m_2} d\xi_{m_3} d\xi_4.$$

Using the integral rule (53) for the space-time face $\mathcal{S}^m$ and relation (52) we find for an integrable $\mathbb{R}^4$-valued function f on $\mathcal{S}_m$:

$$\begin{aligned}\int_{\mathcal{S}_m}\sum_{k=1}^{4} f_k n_k dx =& s\int_{\hat{\mathcal{S}}}\frac{1}{2}\Delta t\sum_{k=1}^{3} f_k\left(\frac{\partial F_{S_m(t)}}{\partial\xi_{m_2}}\wedge\frac{\partial F_{S_m(t)}}{\partial\xi_{m_3}}\right)_k d\xi_{m_2}d\xi_{m_3}d\xi_4\\ &-s\int_{\hat{\mathcal{S}}}\frac{1}{2}f_4\sum_{k=1}^{3}\Delta x_k\left(\frac{\partial F_{S_m(t)}}{\partial\xi_{m_2}}\wedge\frac{\partial F_{S_m(t)}}{\partial\xi_{m_3}}\right)_k d\xi_{m_2}d\xi_{m_3}d\xi_4\\ =&s\frac{1}{2}\Delta t\left(\int_{\hat{\mathcal{S}}}\overline{f}\cdot d\overline{\mathcal{S}}^m-\int_{\hat{\mathcal{S}}}f_4 v\cdot d\overline{\mathcal{S}}^m\right)\\ =&\Delta t\left(\int_{\mathcal{S}_m}\overline{f}\cdot\bar{n}dx-\int_{\mathcal{S}_m}f_4 v\cdot\bar{n}dx\right).\end{aligned}$$

Hence the geometric face integrals containing the space normal and grid velocity are evaluated as follows:

$$\int_{\mathcal{S}_m}\phi_l\phi_k\bar{n}dx = s\frac{1}{2}\Delta t\int_{\hat{\mathcal{S}}}\xi_l\xi_k d\overline{\mathcal{S}}^m, \tag{54}$$

$$\int_{\mathcal{S}_m}\phi_l\phi_k v dx = s\frac{1}{2}\Delta t\int_{\hat{\mathcal{S}}}\xi_l\xi_k\frac{\Delta x}{\Delta t}\cdot d\overline{\mathcal{S}}^m \tag{55}$$

For the face $\mathcal{S}_7$ the parametrization is given by $F(\xi)=(t_n,F_K(\bar{\xi}))$ for $K=K(t_n^+)$. A simple computation shows that for this face we have

$$d\hat{\mathcal{S}}^7 = -|J_K|e_4 d\bar{\xi},$$

where $e_4=(0,0,0,1)^T$ is the last unit vector in $\mathbb{R}^4$. Hence,

$$\int_{\hat{\mathcal{S}}} f\cdot d\hat{\mathcal{S}}^7 = -\int_{\hat{\mathcal{S}}} f_4|J_K|d\bar{\xi} = -\int_{K(t_n^+)} f_4 dx.$$

Likewise we have

$$\int_{\hat{\mathcal{S}}} f\cdot d\hat{\mathcal{S}}^8 = \int_{K(t_{n+1}^-)} f_4 dx.$$

C Geometric integrals

The parametrization of the space-time face $\mathcal{S}$ is the linear interpolation in time of the isoparametric parametrization of the space faces $S^n = S(t_n)$ and $S^{n+1} = S(t_{n+1})$. Let $x_1^n, \ldots, x_4^n$ be the four vertices of the face S^n. Then the isoparametric mapping of S^n is given by

$$\begin{aligned} F_{S^n} : (\xi_1, \xi_2) \mapsto & \hat{x}_1^n + \hat{x}_2^n \xi_1 + \hat{x}_3^n \xi_2 + \hat{x}_4^n \xi_1 \xi_2 \\ := & \frac{1}{4}(x_1 + x_2 + x_3 + x_4) + \frac{1}{4}(-x_1 + x_2 - x_3 + x_4)\xi_1 + \\ & \frac{1}{4}(-x_1 - x_2 + x_3 + x_4)\xi_2 + \frac{1}{4}(x_1 - x_2 - x_3 + x_4)\xi_1\xi_2. \end{aligned} \tag{56}$$

Define the vectors (in $\mathbb{R}^3$)

$$\begin{aligned} a_{00}^n =& \hat{x}_2^n \wedge \hat{x}_3^n = \frac{1}{8}(x_1^n - x_4^n) \wedge (x_2^n - x_3^n), \\ a_{10}^n =& \hat{x}_2^n \wedge \hat{x}_4^n = \frac{1}{8}(x_3^n - x_4^n) \wedge (x_2^n - x_1^n), \\ a_{01}^n =& \hat{x}_4^n \wedge \hat{x}_3^n = \frac{1}{8}(x_1^n - x_3^n) \wedge (x_4^n - x_2^n), \\ c_{00} =& \hat{x}_2^{n+1} \wedge \hat{x}_3^n + \hat{x}_2^n \wedge \hat{x}_3^{n+1} \\ c_{10} =& \hat{x}_2^{n+1} \wedge \hat{x}_4^n + \hat{x}_2^n \wedge \hat{x}_4^{n+1} \\ c_{01} =& \hat{x}_4^{n+1} \wedge \hat{x}_3^n + \hat{x}_4^n \wedge \hat{x}_3^{n+1} \\ n_{00} =& a_{00}^{n+1} + a_{00}^n + \frac{1}{2}c_{00}, \\ n_{10} =& a_{10}^{n+1} + a_{10}^n + \frac{1}{2}c_{10}, \\ n_{01} =& a_{01}^{n+1} + a_{01}^n + \frac{1}{2}c_{01}, \\ d_{00} =& a_{00}^{n+1} - a_{00}^n, \\ d_{10} =& a_{10}^{n+1} - a_{10}^n, \\ d_{01} =& a_{01}^{n+1} - a_{01}^n. \end{aligned} \tag{57}$$

We find

$$\begin{aligned} \frac{\partial F_{S(t)}}{\partial \xi_{m_2}} \wedge \frac{\partial F_{S(t)}}{\partial \xi_{m_3}} =& \frac{1}{4}(1 + \xi_4)^2 (a_{00}^{n+1} + \xi_{m_2} a_{10}^{n+1} + \xi_{m_3} a_{01}^{n+1}) \\ & + \frac{1}{4}(1 - \xi_4)^2 (a_{00}^n + \xi_{m_2} a_{10}^n + \xi_{m_3} a_{01}^n) \\ & + \frac{1}{4}(1 - \xi_4^2)(c_{00} + \xi_{m_2} c_{10} + \xi_{m_3} c_{01}), \end{aligned} \tag{58}$$

and the geometric integrals (54) obtained using this formula are tabulated in Table 2.

Table 2 The integrals $\frac{s}{\Delta t}\int_{\mathcal{S}} \phi_l \phi_m \overline{n} dx$. The sign for $m = m_1$ is equal to $\phi_{m_1|\mathcal{S}}$.

	$m=0$	$m=m_1$	$m=m_2$	$m=m_3$	$m=4$
$l=0$	$\frac{4}{3}n_{00}$	$\pm\frac{4}{3}n_{00}$	$\frac{4}{9}n_{10}$	$\frac{4}{9}n_{01}$	$\frac{2}{3}d_{00}$
$l=m_2$	$\frac{4}{9}n_{10}$	$\pm\frac{4}{9}n_{10}$	$\frac{4}{9}n_{00}$	0	$\frac{2}{9}d_{10}$
$l=m_3$	$\frac{4}{9}n_{01}$	$\pm\frac{4}{9}n_{01}$	0	$\frac{4}{9}n_{00}$	$\frac{2}{9}d_{01}$
$l=4$	$\frac{2}{3}d_{00}$	$\pm\frac{2}{3}d_{00}$	$\frac{2}{9}d_{10}$	$\frac{2}{9}d_{01}$	$\frac{8}{15}n_{00}-\frac{2}{15}c_{00}$

Table 3 The integrals $\frac{s}{\Delta t}\int_{\mathcal{S}} \phi_l \phi_m \overline{n}\cdot v dx$. The sign for $m = m_1$ is equal to $\phi_{m_1|\mathcal{S}}$.

	$m=0$	$m=m_1$	$m=m_2$	$m=m_3$	$m=4$
$l=0$	v_{000}	$\pm v_{000}$	v_{100}	v_{010}	v_{001}
$l=m_2$	v_{100}	$\pm v_{100}$	v_{200}	v_{110}	v_{101}
$l=m_3$	v_{010}	$\pm v_{010}$	v_{110}	v_{020}	v_{011}
$l=4$	v_{001}	$\pm v_{001}$	v_{101}	v_{011}	v_{002}

The grid velocity v is given by

$$v = \frac{\Delta x}{\Delta t} = \hat{b}_1 + \hat{b}_2\xi_{m_2} + \hat{b}_3\xi_{m_3} + \hat{b}_4\xi_{m_2}\xi_{m_3}, \tag{59}$$

with $\hat{b}_i = (\hat{x}_i^{n+1} - \hat{x}_i^n)/\Delta t$. Note that the grid velocity does not depend on the computational time coordinate.

Define the numbers

$$\begin{aligned}
v_{000} &= \tfrac{4}{3}\ \hat{b}_1\cdot n_{00} + \tfrac{4}{9}\ \hat{b}_2\cdot n_{10} + \tfrac{4}{9}\ \hat{b}_3\cdot n_{01},\\
v_{100} &= \tfrac{4}{9}\ \hat{b}_2\cdot n_{00} + \tfrac{4}{9}\ \hat{b}_1\cdot n_{10} + \tfrac{4}{27}\ \hat{b}_4\cdot n_{01},\\
v_{010} &= \tfrac{4}{9}\ \hat{b}_3\cdot n_{00} + \tfrac{4}{27}\ \hat{b}_4\cdot n_{10} + \tfrac{4}{9}\ \hat{b}_1\cdot n_{01},\\
v_{200} &= \tfrac{4}{9}\ \hat{b}_1\cdot n_{00} + \tfrac{4}{15}\ \hat{b}_2\cdot n_{10} + \tfrac{4}{27}\ \hat{b}_3\cdot n_{01},\\
v_{020} &= \tfrac{4}{9}\ \hat{b}_1\cdot n_{00} + \tfrac{4}{27}\ \hat{b}_2\cdot n_{10} + \tfrac{4}{15}\ \hat{b}_3\cdot n_{01},\\
v_{110} &= \tfrac{4}{27}\ \hat{b}_4\cdot n_{00} + \tfrac{4}{27}\ \hat{b}_3\cdot n_{10} + \tfrac{4}{27}\ \hat{b}_2\cdot n_{01},\\
v_{001} &= \tfrac{2}{3}\ \hat{b}_1\cdot d_{00} + \tfrac{2}{9}\ \hat{b}_2\cdot d_{10} + \tfrac{2}{9}\ \hat{b}_3\cdot d_{01},\\
v_{101} &= \tfrac{2}{9}\ \hat{b}_2\cdot d_{00} + \tfrac{2}{9}\ \hat{b}_1\cdot d_{10} + \tfrac{2}{27}\ \hat{b}_4\cdot d_{01},\\
v_{011} &= \tfrac{2}{9}\ \hat{b}_3\cdot d_{00} + \tfrac{2}{27}\ \hat{b}_4\cdot d_{10} + \tfrac{2}{9}\ \hat{b}_1\cdot d_{01},\\
v_{002} &= \tfrac{8}{15}\ \hat{b}_1\cdot n_{00} + \tfrac{8}{45}\ \hat{b}_2\cdot n_{10} + \tfrac{8}{45}\ \hat{b}_3\cdot n_{01}\\
&\quad - \tfrac{2}{15}\ \hat{b}_1\cdot c_{00} - \tfrac{2}{45}\ \hat{b}_2\cdot c_{10} - \tfrac{2}{45}\ \hat{b}_3\cdot c_{01}.
\end{aligned}$$

Using these expressions the integrals (55) are computed and tabulated in Table 3.

D Discrete conservation

In order to stay conservative at the discrete level, the face fluxes are computed for one cell connecting to the face, and added to the other cell using only some permutation relations. These relations are the generalization of the principle that for general finite volume schemes the flux added to the one connecting cell is substracted from the other.

Let $\mathcal{S}$ connect the cells $\mathcal{K}$ and $\mathcal{K}'$. The local face coordinate system $(\xi'_{m'_2}, \xi'_{m'_3}, \xi'_4)$ of the face derived from the topology of cell $\mathcal{K}'$ is connected with the coordinate system $(\xi_{m_2}, \xi_{m_3}, \xi_4)$ through:

$$\begin{pmatrix} \xi'_{m'_2} \\ \xi'_{m'_3} \\ \xi'_4 \end{pmatrix} = \begin{pmatrix} A_i & 0 \\ 0 & 1 \end{pmatrix} \begin{pmatrix} \xi_{m_2} \\ \xi_{m_3} \\ \xi_4 \end{pmatrix}, \qquad 1 \le i \le 8, \tag{60}$$

where A_i is one of the eight following rotation/mirror matrices:

$$A_1 = \begin{pmatrix} 1 & 0 \\ 0 & 1 \end{pmatrix}, \quad A_2 = \begin{pmatrix} 0 & 1 \\ -1 & 0 \end{pmatrix}, \quad A_3 = \begin{pmatrix} -1 & 0 \\ 0 & -1 \end{pmatrix}, \quad A_4 = \begin{pmatrix} 0 & -1 \\ 1 & 0 \end{pmatrix},$$
$$A_5 = \begin{pmatrix} -1 & 0 \\ 0 & 1 \end{pmatrix}, \quad A_6 = \begin{pmatrix} 0 & 1 \\ 1 & 0 \end{pmatrix}, \qquad A_7 = \begin{pmatrix} 1 & 0 \\ 0 & -1 \end{pmatrix}, \quad A_8 = \begin{pmatrix} 0 & -1 \\ -1 & 0 \end{pmatrix}.$$

Let m_i, resp. m'_i, $(1 \le i \le 3)$ be the ordering of the space gradients in cell $\mathcal{K}$, resp. $\mathcal{K}'$, such that (compare with (17))

$$U^{\mathcal{K}}_{|\mathcal{S}}(\xi_{m_2}, \xi_{m_3}, \xi_4) = U(\bar{\xi}_{m_1}; \mathcal{K}) + \xi_{m_2}\hat{U}_{m_2}(\mathcal{K}) + \xi_{m_3}\hat{U}_{m_3}(\mathcal{K}) + \xi_4\hat{U}_4(\mathcal{K})$$
$$U^{\mathcal{K}'}_{|\mathcal{S}}(\xi'_{m_2}, \xi'_{m_3}, \xi'_4) = U(\bar{\xi}_{m'_1}; \mathcal{K}') + \xi'_{m'_2}\hat{U}_{m'_2}(\mathcal{K}') + \xi'_{m'_3}\hat{U}_{m'_3}(\mathcal{K}') + \xi'_4\hat{U}_4(\mathcal{K}').$$

Using (60) we find that in the computational coordinates of face $\mathcal{S}$ the latter equality is equivalent with

$$U^{\mathcal{K}'}_{|\mathcal{S}}(\xi_{m_2}, \xi_{m_3}, \xi_4) = U(\bar{\xi}_{m'_1}; \mathcal{K}') + \xi_{m_2}\hat{U}'_{m_2}(\mathcal{K}') + \xi_{m_3}\hat{U}'_{m_3}(\mathcal{K}') + \xi_4\hat{U}_4(\mathcal{K}').$$

where the transversal gradients are defined by

$$\begin{pmatrix} \hat{U}'_{m_2}(\mathcal{K}') \\ \hat{U}'_{m_3}(\mathcal{K}') \end{pmatrix} = A_i^T \begin{pmatrix} \hat{U}_{m'_2}(\mathcal{K}') \\ \hat{U}_{m'_3}(\mathcal{K}') \end{pmatrix}.$$

By definition of the basis functions, (60) implies

$$\begin{pmatrix} \phi^{\mathcal{K}'}_{m'_2|\mathcal{S}} \\ \phi^{\mathcal{K}'}_{m'_3|\mathcal{S}} \end{pmatrix} = A_i \begin{pmatrix} \phi^{\mathcal{K}}_{m_2|\mathcal{S}} \\ \phi^{\mathcal{K}}_{m_3|\mathcal{S}} \end{pmatrix}.$$

The remaining basis function is constant on the face: $\phi^{\mathcal{K}}_{m_1|\mathcal{S}} = s_{\mathcal{S}}$ and $\phi^{\mathcal{K}'}_{m'_1|\mathcal{S}} = s'_{\mathcal{S}}$.

The numerical flux is consistent, and hence

$$F_{\mathrm{HLLC}}(U_R, U_L, \overline{n}) = -F_{\mathrm{HLLC}}(U_L, U_R, -\overline{n}).$$

Let U'_L and U'_R be the left and right states as seen from cell $\mathcal{K}'$ and let $\overline{n}'$ be the outward pointing normal of face $\mathcal{S}$ for cell $\mathcal{K}'$. Then,

$$\begin{aligned}
\int_{\mathcal{S}} F_{\mathrm{HLLC}}(U'_L, U'_R, \overline{n}')dx &= \int_{\mathcal{S}} F_{\mathrm{HLLC}}(U_R, U_L, -\overline{n})dx \\
&= -\int_{\mathcal{S}} F_{\mathrm{HLLC}}(U_L, U_R, \overline{n})dx, \\
\int_{\mathcal{S}} \phi^{\mathcal{K}'}_{m'_1} F_{HLLC}(U'_L, U'_R, \overline{n}')dx &= -s'_{\mathcal{S}} \int_{\mathcal{S}} F_{\mathrm{HLLC}}(U_L, U_R, \overline{n})dx, \\
\int_{\mathcal{S}} \begin{pmatrix} \phi^{\mathcal{K}'}_{m'_2} \\ \phi^{\mathcal{K}'}_{m'_3} \end{pmatrix} F_{\mathrm{HLLC}}(U'_L, U'_R, \overline{n}') &= -A_i \int_{\mathcal{S}} \begin{pmatrix} \phi^{\mathcal{K}}_{m_2} \\ \phi^{\mathcal{K}}_{m_3} \end{pmatrix} F_{\mathrm{HLLC}}(U_L, U_R, \overline{n})dx, \\
\int_{\mathcal{S}} \phi^{\mathcal{K}'}_4 F_{\mathrm{HLLC}}(U'_L, U'_R, \overline{n}')dx &= -\int_{\mathcal{S}} \phi^{\mathcal{K}}_4 F_{\mathrm{HLLC}}(U_L, U_R, \overline{n})dx.
\end{aligned} \tag{61}$$

So, the face fluxes for cell $\mathcal{K}'$ easily follow from the fluxes for cell $\mathcal{K}$.